



# 1 Main Ethiopian Rift landslides formed in contrasting geological 2 settings and climatic conditions

3  
4 Karel Martínek\*<sup>1,2</sup>, Kryštof Verner<sup>2,3</sup>, Tomáš Hroch<sup>2</sup>, Leta A. Megerssa<sup>3,2</sup>, Veronika  
5 Kopačková<sup>2</sup>, David Buriánek<sup>2</sup>, Ameha Muluneh<sup>4</sup>, Radka Kalinová<sup>3</sup>, Miheret Yakob<sup>5</sup>, Muluken  
6 Kassa<sup>4</sup>

7 \*corresponding author

8 <sup>1</sup> Institute of Geology and Palaeontology, Faculty of Science, Charles University, Albertov 6,  
9 Prague, 12843, Czech Republic (karel.j.martinek@gmail.com)

10 <sup>2</sup> Czech Geological Survey, Klárov 3, 118 21 Prague, Czech Republic

11 <sup>3</sup> Institute of Petrology and Structural Geology, Faculty of Science, Charles University, Albertov 6, Prague, 12843,  
12 Czech Republic

13 <sup>4</sup> School of Earth Sciences, Addis Ababa University, Arat Kilo, 1176, Addis Ababa, Ethiopia

14 <sup>5</sup> Geological Survey of Ethiopia, CMC road, Bole Keb.10/Wor.6, POBox: 2302, Addis Ababa, Ethiopia

15  
16 **Abstract.** The Main Ethiopian Rift (MER), where active continental rifting creates specific conditions for landslide  
17 formation, provides a prospective area to study the influence of tectonics, lithology, geomorphology, and climate on  
18 landslide formation. New structural and morphotectonic data from CMER and SMER support a model of  
19 progressive change in the regional extension from NW – SE to the recent E(ENE) – W(WSW) direction driven by  
20 the African and Somalian plates moving apart with the presumed contribution of the NNE(NE) – SSW(SW)  
21 extension controlled by the Arabic Plate. The formation and polyphase reactivation of faults in the changing regional  
22 stress-field significantly increase the rocks' tectonic anisotropy and the risk of slope instabilities forming.  
23 According to geostatistical analysis landslides in the central and southern MER occur on steep slopes, almost  
24 exclusively formed on active normal fault escarpments. Landslides are also influenced by higher annual  
25 precipitation, precipitation seasonality, vegetation density and seasonality.  
26 A detailed study on active rift escarpment in the Arba Minch area revealed similar affinities as in regional study of  
27 MER. Landslides here are closely associated with steep, mostly faulted, slopes and a higher density of vegetation.  
28 Active tectonics and seismicity are the main triggers. The Mejo area situated on the uplifting Ethiopian Plateau 60  
29 km east of the Rift Valley shows that landslide occurrence is strongly influenced by steep erosional slopes and  
30 deeply weathered Proterozoic metamorphic basement. Rapid headward erosion, unfavourable lithological conditions  
31 and more intense precipitation and higher precipitation seasonality are the main triggers here.  
32

## 33 **Keywords:**

34 Landslides, Main Ethiopian Rift (MER), morphotectonics, tectonics, geological setting, climate, geostatistics

## 36 **1. Introduction**

37 Slope instabilities including mainly landslides, rockfalls and debris flows are usually influenced by key factors such  
38 as geomorphology, bedrock lithology and rock fabric anisotropy, active tectonics and seismicity, type and grade of  
39 weathering, climatic conditions, vegetation cover, land use and human activity. Links between these factors and the  
40 formation of landslides and rockfalls are complex (e.g. Abebe et al., 2010; Meinhardt et al., 2015). Geomorphic  
41 indices have been used to decipher links between landform and tectonics in several studies (Ayalew and Yamagishi,  
42 2004; Ayalew et al., 2004). However, the influence of other factors on slope instabilities is unclear and a matter of  
43 current debate (e.g. Asfaw, 2007; Temesgen et al., 1999; Vařilová et al., 2015; Woldearegay, 2013). In general,  
44 ongoing discussions on the formation of slope instabilities in an active rift setting state either tectonics, climate or  
45 anthropogenic activity as triggering factors depending on the characteristic conditions at the particular locality (e.g.  
46 Mancini et al., 2010; Peduzzi, 2010; Wotchoko et al., 2016). Other studies also conclude that lithology and  
47 precipitation are the main landslide controlling factors (e.g. Kumar et al. 2019; and references therein).  
48 Geomorphic indices, such as slope, aspect, hypsometric integral, the stream length gradient index or river incision  
49 rates, are capable of detecting landform responses to tectonics (Ayalew and Yamagishi, 2004; Gao et al., 2013) but  
50 studies showing slope instabilities having a direct link to active tectonics are relatively rare (Chang et al., 2018 and  
51 references therein). Other studies also conclude that lithology and precipitation are main landslide controlling factors  
52 (e.g. Kumar et al. 2019 and references therein).



53 Central and southern parts of the Main Ethiopian Rift (MER), which belong to the northern part of the East African  
54 Rift System (EARS), form a relatively narrow, slowly spreading extensional zone with a humid, strongly seasonal  
55 climate. There is a thick sequence of unconsolidated, often strongly weathered volcanoclastic deposits cropping out  
56 in grabens, on steep tectonic slopes or occasionally also on moderately elevated areas. Such a complex environment  
57 is an excellent natural laboratory to study the interplay of factors influencing various types of slope instabilities as  
58 they form in different geological and geomorphic conditions. Active extensional tectonism has a strong influence on  
59 the present-day morphology, but there are also important variations in climatic parameters (annual precipitation,  
60 seasonality); moreover, a population explosion in the last decades has led to extensive deforestation, overgrazing  
61 and dramatic changes of landcover and land use, which all may have significant importance in landslide formation  
62 (FAO 2001; Janetos and Justice, 2000; Gessesse, 2007; Gete and Hurni, 2001; Melese 2016).  
63 This multidisciplinary study is focused on evaluating the landslide distribution in the central and southern MER. A  
64 combination of the results of geological, geohazard and structural mapping, with remotely sensed data, and climatic,  
65 vegetation and land use indicators is assessed using geostatistical methods. The discussion of the main factors  
66 influencing the formation of landslides in the regional scale in the central and southern MER and also on a detailed  
67 scale in the Mejo and Arba Minch areas in the southern part of the MER is the main focus of this study. In regional  
68 scale study the direct link to tectonics is clear, so we present large dataset of new field structural data from this area.  
69 The situation in detailed scale studies in Mejo and Arba Minch is more complex. These two areas have contrasting  
70 styles of tectonic setting and varying lithological and climatic conditions: the Mejo landslide area is more humid,  
71 located on the eastern plateau, 60 km east of the rift valley and dominated by highly weathered Proterozoic  
72 basement rocks, while the Arba Minch landslide area is situated directly on the western rift escarpment with active  
73 tectonism and seismicity, and dominated by Tertiary volcanic rocks (Fig. 1). In both areas, slope failures are closely  
74 associated with steep slopes, but these are generated by very different processes – either active rift normal faulting  
75 or deep head-ward river erosion of uplifting rift flank. The anthropogenic influence is also discussed, but only  
76 locally, because the relevant data for a thorough geostatistical evaluation are unfortunately missing.

77

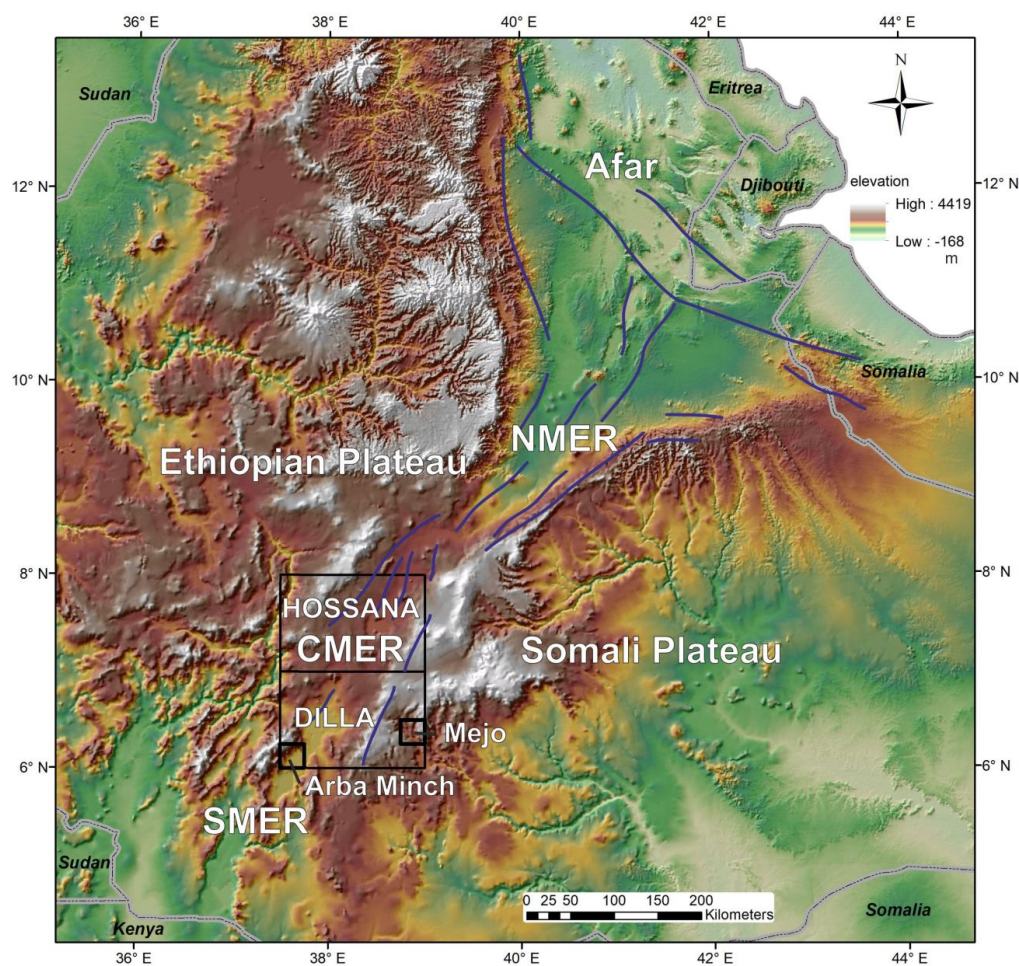
## 78 **2. Geological and geohazard setting**

### 79 **2.1. Geology and tectonics of the studied area**

80 The overall geological pattern of the southern Ethiopia includes a basement formed by metamorphic rocks of the  
81 Neoproterozoic age, which have been overlaid by widespread volcanic sequences ranging from pre-rift Cenozoic  
82 volcanism to the Main Ethiopian Rift (MER) associated volcanism (Bonini et al., 2005; Hayward and Ebinger, 1996;  
83 Woldegabriel et al., 2000). The Precambrian rocks exposed in southern Ethiopia constitute the most southern part of  
84 the Arabian-Nubian Shield (ANS) which includes several terrane assemblages (for a review see Fritz et al. 2013 and  
85 references therein). The ANS is an assemblage of juvenile low-grade volcano-sedimentary rocks and associated  
86 plutons and ophiolite traces with ages between ~890 and 580 Ma (Fritz et al., 2013). The Main Ethiopian Rift  
87 (MER), is an active intra-continental rift bearing magma-dominated extension of the African (Nubian), Somalian,  
88 and Arabian lithospheric plates (e.g. Acocella, 2010; Agostini et al., 2011). Three segments of the MER reflecting  
89 temporally and spatially different stages of regional extension and volcanic activity have been defined (e.g. Hayward  
90 and Ebinger, 1996; Mulunch et al., 2014): (a) the Northern Main Ethiopian Rift (NMER), (b) the Central Main  
91 Ethiopian Rift (CMER) and (c) the Southern Main Ethiopian Rift (SMER, see Fig. 1). In the southern part of the  
92 MER, the current rate of ~E – W oriented extension between the African and Somalian plates amounts 5.2±0.9  
93 mm/yr (Saria et al., 2014).  
94 The volcanic activity in the studied parts of the CMER (Hossana Area) and SMER (Dilla Area) could be divided  
95 into three major episodes (Bonini et al., 2005; Corti, 2009; Hayward and Ebinger, 1996). The Eocene to Oligocene  
96 pre-rift volcanic products (~45 to 27 Ma) comprise mainly tholeiite to alkaline basalt lava flows and the associated  
97 volcanoclastic deposits (Amaro-Gamo Basalts) with the presence of rhyolite ignimbrites (Shole Ignimbrites) and  
98 minor trachytes (Burianek et al., 2018; Verner et al., 2018b; Verner et al., 2018d). The Miocene syn-rift volcanic  
99 products (~22 to 8 Ma) are represented by basalts, felsic volcanites and volcanoclastic rocks (rhyolite lava, minor  
100 ignimbrites, trachyte lava flows and related pyroclastic deposits) belonging mainly to the Getra and Kele sequences  
101 including Mimo trachyte (Bonini et al., 2005; Ebinger et al., 1993; Ebinger et al., 2000). These two events were  
102 followed by a period of drastically low volcanism except for a small eruption of peralkaline pantelleritic ignimbrites  
103 intercalated with minor basaltic lava flows in the areas beyond the rift escarpments (Bonini et al., 2005; see also Fig.  
104 4). Subsequently, the products of Pleistocene to Holocene post-rift volcanic activity (~1.6 – 0.5 Ma) are bi-modal  
105 volcanites and volcanoclastic rocks such as, for example, massive Nech-Sar basalts, rhyolites, strongly welded  
106 rhyolitic ignimbrites and other pyroclastic deposits (Ebinger et al., 1993). A typical example of post-rift volcanic



107 activity in the southern CMER is the lower Pleistocene formation of unconsolidated pyroclastic deposits on the rift  
108 floor (e.g. Corbetti Volcanic System, Rapprich et al., 2014), which was consequently disturbed by tectonic  
109 movements and erosion.  
110 The complex fault pattern of the MER (interference of SSW(SW) -NNE(NE), N-S and WNW(W) -ESE(E) trending  
111 faults) has been attributed to various mechanisms of contrasting hypothesis (for a review see Abate et al., 2015;  
112 Erbello and Kidane, 2018): (a) The pure extension orthogonal to the rift; (b) a right-lateral NW – SE to the NNW –  
113 ESE transtension continuously transferred to sinistral oblique rifting as a result of an E – W regional extension; (c) a  
114 constant NE(ENE) – SW(WSW) trending extension; (d) constant extension in the NW – SE direction and (e)  
115 constant E – W to ESE – WNW extension.  
116



117  
118 *Fig. 1 The Hossana and Dilla areas in the central and southern part of the Main Ethiopian Rift (MER). The location*  
119 *of the NMER (northern MER), CMER (central MER), SMER (southern MER) and Mejo and Arba Minch case study*  
120 *areas are also indicated. The blue lines represent major fault zones.*

121  
122 **2.2. Geohazards in the central and southern MER**

123 Notable geohazard features across and along the MER range from intense erosion to slope instability-related mass  
124 wasting processes including rock falls, debris flows up to shallow and deep-seated landslides, all with immense  
125 costs in terms of casualty and infrastructure loss (Abebe et al., 2005; Ayalew, 1999; Hearn, 2018). Landslides are  
126 rather more common in the highlands of Ethiopia. The most affected regions are the Blue Nile Gorge (Ayalew and



127 Yamagishi, 2004; Gezahegn and Dessie, 1994; JICA and GSE, 2012; Tadesse, 1993), the Dessie area and the  
128 highlands surrounding Ambassel and Woldia (Ayenew and Barbieri, 2005; Fubelli et al., 2008), the Semien  
129 highlands, particularly western and central Tigray, the Sawla and Bonga areas of south Ethiopia (Lemessa et al.,  
130 2000) and the MER margins of the western and eastern escarpment (Kycl et al., 2017; Rappich and Eshetu, 2014;  
131 Rappich et al., 2014; Temesgen et al., 2001), the surroundings of Finchewa and the Debre Libanos and the Mughher  
132 locality (Zvelebil et al., 2010). On the western escarpment of the MER, a vast and recurrent landslide is notable  
133 close to the town of Debre Sina at the locality of Yizeba Weyn in central Ethiopia (Kropáček et al., 2015).  
134 Other common geological hazards that recurrently appear in the area are ground fissures in various sectors along the  
135 rift floor. For example, north of the Fentale area in the northern MER (Williams et al., 2004) and various localities  
136 in the central MER segment (Asfaw, 1982; Asfaw, 1998; Ayalew et al., 2004) which often transform into deep and  
137 long gully systems (Billi and Dramis, 2003). Persistent seismic tremors, usually of lower magnitudes, are apparently  
138 located in the entire rift floor (e.g. Wilks et al., 2017). Particular clusters and source zones have been identified in  
139 Ethiopia those being (1) the western plateau margin, (2) the central Afar, (3) the Aisha block, (4) the Ankober area,  
140 (5) the central Main Ethiopian Rift and (6) the South Western Main Ethiopian Rift (Ayele, 2017). Nevertheless,  
141 historical high magnitude earthquake records have also been reported (Asfaw, 1992; Gouin, 1975; Gouin, 1979;  
142 Wilks et al., 2017). An updated probabilistic seismic hazard analysis and zonation has since been recently carried  
143 out with seismotectonic source zones constrained from recent studies for the Horn of Africa with reference to the  
144 East African Rift Valley (Ayele, 2017).

145 In addition to the seismic tremors, volcanism is also of apparent risk. Among the recent events are the Nabro  
146 Volcano in 2011 in the far northern part of the Afar triangle (Goitom et al., 2015) and the Debahu rifting and  
147 volcanic dyke swarm intrusion events in 2005 (Ayele et al., 2007; Ayele et al., 2009). These two events each  
148 triggered major alarms significant enough to warrant flight diversions (in the case of the Nabro volcano) across the  
149 region and the temporary displacement of local people (e.g. Goitom et al., 2015).

150

### 151 3. Methods

152 Field geological, structural, geomorphological and engineering geological mapping were conducted to acquire  
153 geological, tectonic, geomorphological and rock mechanic properties (rock mass strength) characteristics.  
154 Rock mass strength is obtained from the Engineering geological map of Hossana map sheet (Yekoye et al., 2012)  
155 and Dilla map sheet (Habtamu et al., 2012). The maps are prepared based on extensive and multiple types of field  
156 data to classify the lithological units into ranks of strength class as Very Low, Low, Medium, High, Very High rock  
157 mass strength units. These classifications are based on multiple criteria evaluation determined from field  
158 documentation including intact rock strength, discontinuity conditions and degree of weathering. The intact rock  
159 strength determination is made either by Schmidt hammers or testing of representative irregular samples under the  
160 point load tester and the results normalized to standard size of sample as recommended by ISRM (1985) to IS<sub>50</sub>  
161 reference strength. The discontinuity condition is determined by considering the spacing, aperture and discontinuity  
162 surface roughness and overall geometry. The degree of weathering on the other hand is determined qualitatively on  
163 the bases of the criteria set out in British Standard (BS 5930, 1981) from various outcrops in the region.  
164 The precipitation data were obtained from the national database that was set up by the Centre for Development and  
165 Environment (CDE), University of Bern, Switzerland in the 1990's for all of Ethiopia. Since its beginning, the  
166 dataset has been upgraded with additional information layers but the dataset released as version I on a single CD-  
167 ROM, which has mean monthly precipitation data of the major settlement areas with information on the temporal  
168 coverage of recorded years, has been used in this study (CDE, 1999). Precipitation point data (Centre for  
169 Development and Environment, 1999) were averaged (annual, each month) and then the spatial distribution over the  
170 areas of interest were interpolated using the Inverse Distance Weighted method (IDW). Nevertheless, the  
171 precipitation seasonality index could not be calculated due to data inhomogeneities, where only some stations have a  
172 recording period of more than 20 yrs., but often less than 5 yrs. In order to calculate a seasonality index, 30 yrs.  
173 continuity is required. Therefore, precipitation seasonality was evaluated using standard deviation among particular  
174 monthly precipitations and by wet (July + August) and dry season (December + January) differences. Monthly  
175 averages of all available data were considered for calculations.  
176 Aster DEM, SRTM3 and Landsat 7 ETM+ were used for morphotectonic analysis, the vegetation index (NDVI)  
177 based on Modis (Terra Modis, USGS eMODIS Africa 10-Day Composite) and land use / land cover data available  
178 from the U.S. Geological Survey (<https://earthexplorer.usgs.gov/>, 2018) were also evaluated. Modis scenes from  
179 January (peak of dry season) and August (peak of wet season) 2016 were used for the vegetation assessment.



180 The main approach for the morphotectonic analysis followed that used by Dhont and Chorowicz (2006 and  
181 references therein). The main aim was to use DEM imagery to interpret the largest neotectonic structures in the  
182 central and southern MER regions. Single-directional and multi-directional shaded reliefs and an elevation coloured  
183 ASTER DEM image (Fig. 3) was generated using ArcMap 10.6 ([www.esri.com](http://www.esri.com)). This DEM constitutes the basis for  
184 morphotectonic analysis at the regional scale. The faults mapped can be considered as the main neotectonic faults  
185 because they have a prominent expression in the morphology. In some cases they form asymmetric ranges with one  
186 side corresponding to breaks in slope or scarps; by the displacement of Pleistocene and Neogene lithological  
187 boundaries; by the occurrence of straight lines of kilometres to several tens of kilometres in length. The images were  
188 compared with field geological mapping data to distinguish the scarps formed by active faults from those formed by  
189 differential erosion of contrasted lithology.

190 The emplacement of volcanoes, which are abundant in study area, can also be related to tectonic structures such as  
191 tension fractures or open faults. Small volcanoes arranged along the straight lines or linear clusters of adjacent  
192 volcanoes were also interpreted as linear structures. The result of the interpretation is called “linear indices” which  
193 mostly represent active faults (normal and normal-oblique slip), but because of uncertainties in detailed lithology in  
194 some areas and a lack of field verification in some cases, the “linear indices” may also represent prominent fracture  
195 zones, in exceptional cases, also lithological boundaries. To avoid such uncertainties, an independent evaluation of  
196 the geomorphology by numerical methods was carried out. For an evaluation of the main tectonic indications of the  
197 CMER and SMER, morphotectonic analysis was carried out at a regional scale of 1:250 000 (presented in sections  
198 4.1. and 4.4.), while case studies Mejo and Arba Minch were evaluated on a detailed scale of 1: 50 000 (chapter  
199 4.5.).

200 In addition to a visual interpretation of linear indices, a quantitative technique - morphometry - was also employed  
201 to analyse landforms in a quantitative manner. This technique uses numerical parameters such as slope, surface  
202 curvature and convexity to extract morphological and hydrological objects (e.g., stream networks, landforms) from  
203 DEM (Fisher et al., 2004; Pike, 2000; Wood, 1996). Landforms and lithological units reflect also different  
204 geotechnical properties (e.g. rock strength, degree of weathering) so they can be identified by these numerical  
205 methods. Various studies have been carried out to link morphometry with land erosion, tectonics and diverse  
206 geomorphological conditions and volcanic activity (Altin and Altin, 2011; Bolongaro-Crevenna et al., 2005; Ganas  
207 et al., 2005; Kopačková et al., 2011; Rapprich et al., 2010). Morphometric maps were constructed utilizing Wood’s  
208 algorithm based on SRTM DEM data (30 m pixel resolution). First, the topographic slope and the maximum and  
209 minimum convexity values were derived at a pixel by pixel basis. The variation in these parameters was quantified  
210 for each pixel with respect to neighbouring pixels (in orthogonal directions). Secondly, based on a set of tolerance  
211 rules, morphometric classes were defined for each pixel: ridge, channel, plane, peak, pit and pass (Wood, 1996).  
212 Wood’s algorithm allows the relief to be parametrized by setting different values for the tolerance of the topographic  
213 slope and convexity. In this study the slope tolerance of 3.0 and convexity tolerance of 0.02 were used for the best  
214 fit.

215

#### 216 4. Results and interpretations

217 The results of the regional study of morphotectonics, morphometric and field structural analysis, slope failure  
218 mapping and a geostatistical evaluation of the relationships between tectonic, lithological and surface conditions,  
219 and the occurrence of the landslides are presented here. Also, a more detailed evaluation is finally carried out taking  
220 two case study sites at Mejo (on MER eastern shoulder) and Arba Minch (western MER escarpment) areas which  
221 have a contrasting geological and climatic setting across the MER.

222

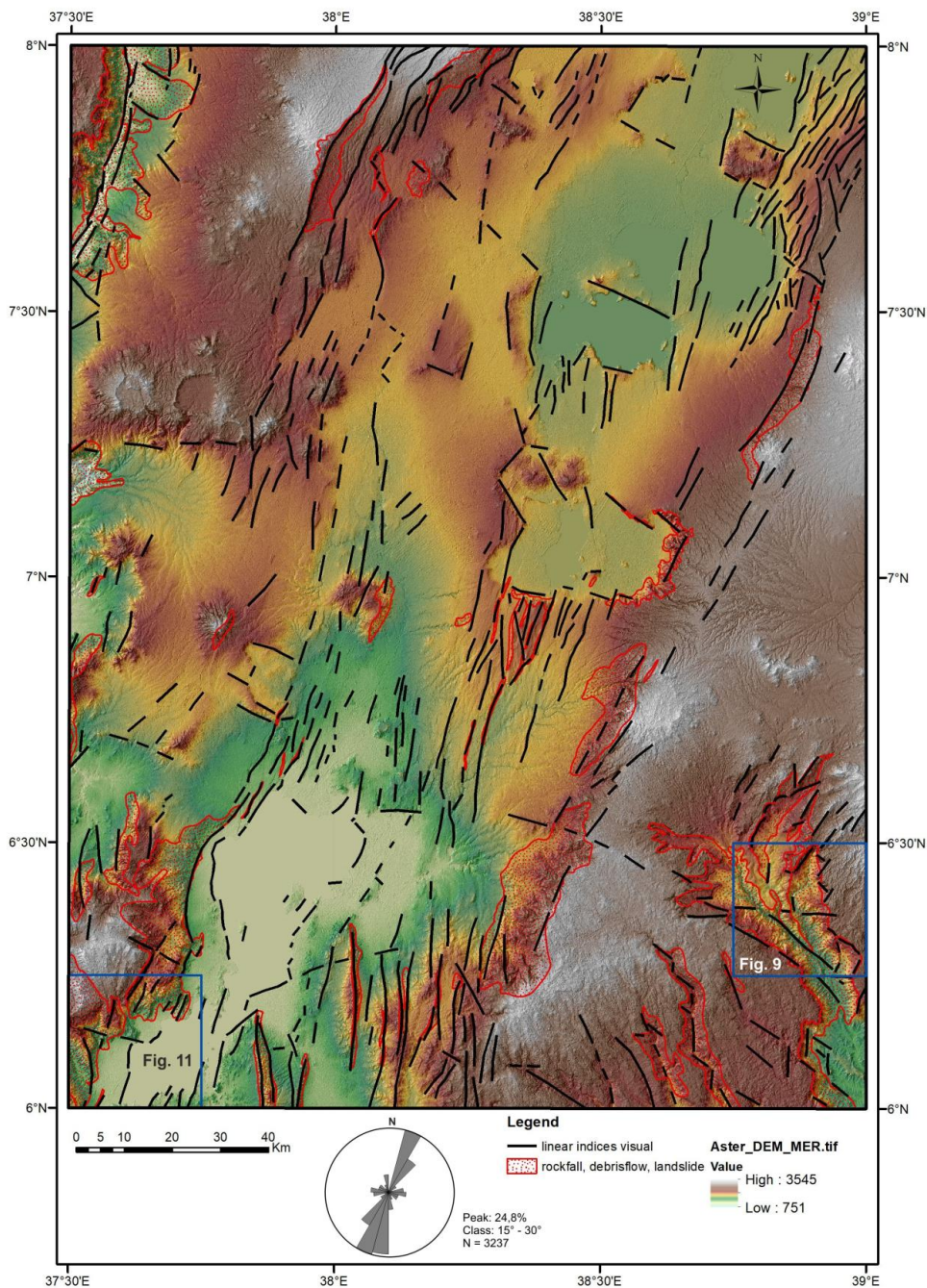
223

##### 224 4.1. Morphotectonic and morphometric analysis

225 Shaded relief maps, derived from DEMs with NW, N and NE illumination, and multidirectional shaded relief maps  
226 were used as a base map for morphotectonic interpretation. After carrying out the first stage of a visual interpretation  
227 of the lineaments, the second stage was carried out on the automated/numerical morphology base map, which helped  
228 uncover some important lineaments with a not so prominent morphological expression. Based on a comparison with  
229 geological maps, lineaments representing lithological boundaries, without evidence of faults, were removed during  
230 the third stage. Thus, the interpreted lineaments mostly represent present-day active faults, fault zones, important  
231 fracture zones and possibly also shear zones (if there are any) which are manifested in morphology. Moreover, older  
232 faults with a prominent lithological contrast can be expressed in morphology. The interpretation was made on a



233 scale of 1:250 000, so only the lineaments considered to represent a main fault or other tectonic zones have been  
234 mapped.  
235



236

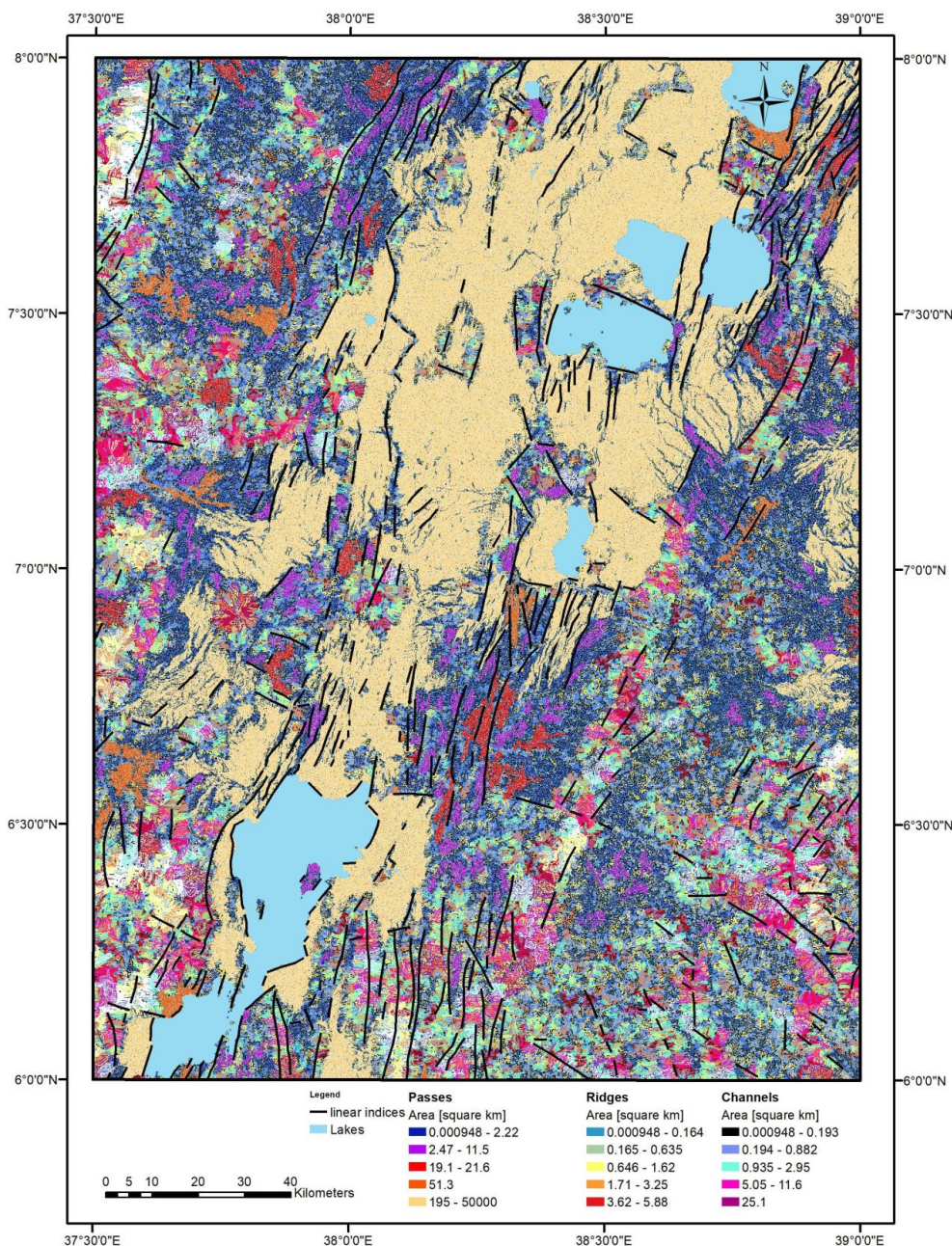


237 *Fig. 2. DEM (colour elevation map on multidirectional shaded relief) of the Dilla and Hossana areas with visually*  
238 *interpreted linear indices and the distribution of their strikes in a rose diagram. The location of the Mejo (Fig. 9)*  
239 *and Arba Minch (Fig. 11) detailed study areas are also shown (see section 4.5).*

240

241 A combination of a visual morphotectonic interpretation based on DEMs (Fig. 2) and an interpretation on  
242 morphometric landforms (Fig. 3) was used to map lineaments. The study area is characterised by a predominance of  
243 NNE-SSW oriented lineaments mostly representing the major normal faults of the rift valley. The central and  
244 northern parts of the study area represent a relatively wider rift zone with extension spread over a larger area, while  
245 the southern part is narrower with steeper topographic gradients and more prominent vertical displacements on the  
246 faults. The subordinate population of lineaments, mostly perpendicular to the strike of the rift has E-W to WNW  
247 trend showing also vertical displacement.

248



249  
250 *Fig. 3. Morphotectonic analysis of the Dilla and Hossana areas based on morphometry. Linear indices show only*  
251 *lines, which are in accordance with both the visual interpretation of the DEM and the morphometry.*  
252

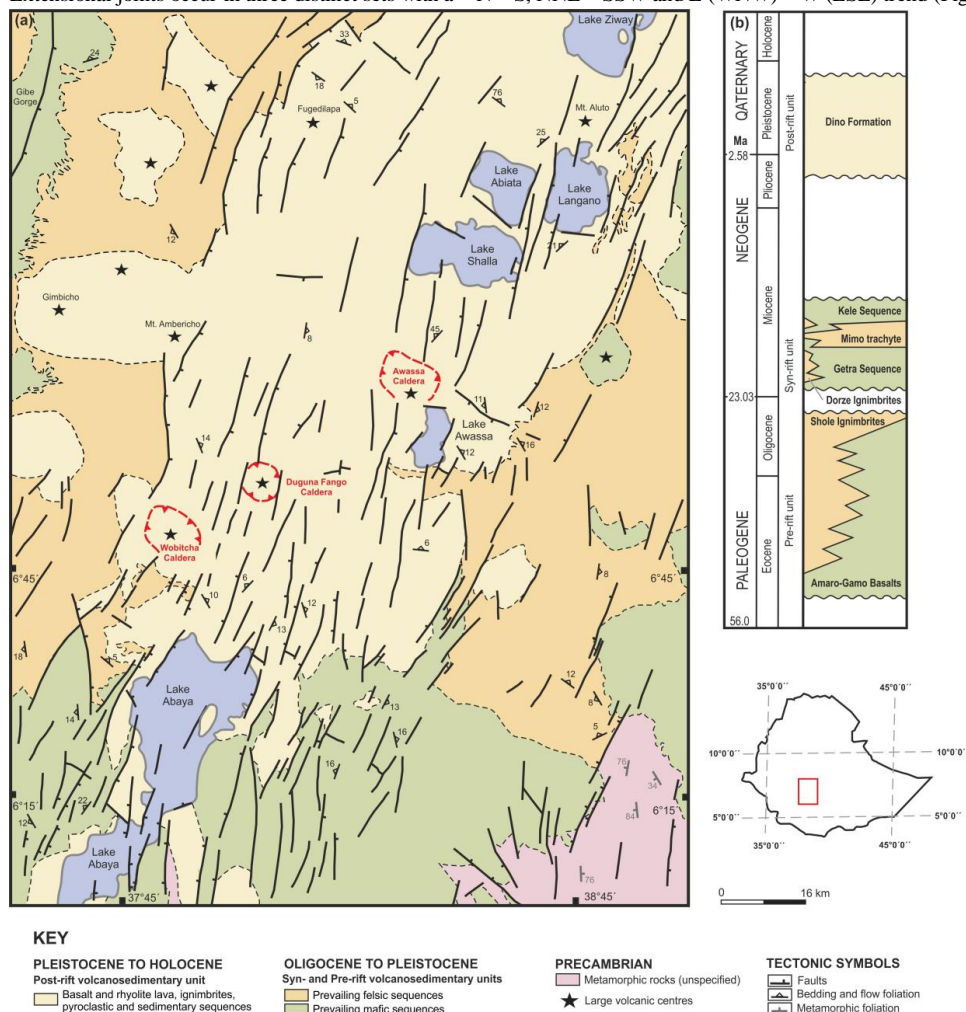
#### 253 4.2. Tectonics

254 The primary fabrics in rift-related volcanic deposits and lava flows are defined by the planar preferred orientation of  
255 rock-forming minerals, micro-vesicles or micro-crystals and elongated mineral grains, lithic fragments or stretched  
256 and welded pumice fragments. With the exception of the lateral parts of lava flows or volcanic centres, these planar





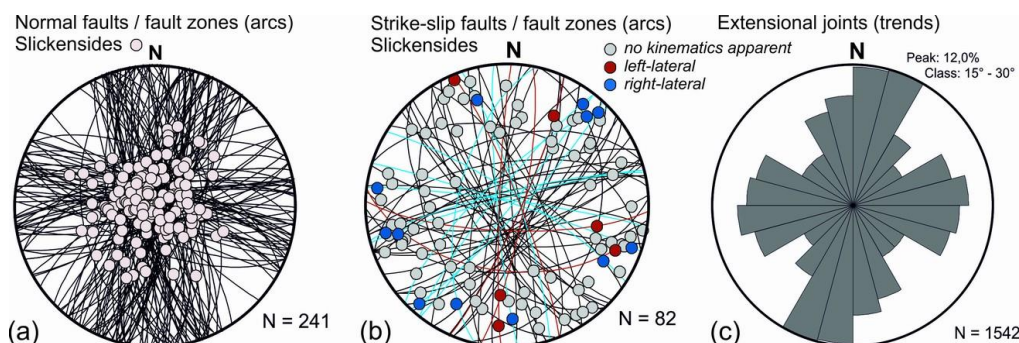
257 fabrics are predominantly flat-lying or dip gently to ~SSW or E. In addition, large amount of fault structures  
 258 associated to the ~NNE-SSW trending MERS dip predominantly steeply to ~ESE in the western part of the rift and  
 259 to ~WNW along its eastern margin. The main ~NNE-SSW trending faults also form a prominent escarpments and  
 260 other morphological features of the MER (Figs. 4 a, 5). These faults are associated with fault lineation (slickensides)  
 261 plunging steeply to moderately to ~SE (in the western escarpment) or to ~NW (in the eastern escarpment), both  
 262 bearing exclusively normal kinematic indicators (Fig. 6 a, b, c). Two subordinate sets of fault structures appear to be  
 263 synchronous with the main ~NNE-SSW faults are mostly perpendicular, WNW(W)-ESE(E) trending normal faults  
 264 with predominantly NNW plunging slickensides or steeply ~NNW dipping normal faults (Fig. 5a). Relatively  
 265 younger or newly reactivated ~NNW(N)-SSE(S) trending faults which are oblique by ~20-30° to the main fault  
 266 system were mapped mainly in the central part of the rift valley (Fig. 2, 5a). In addition, ~NNW – ESE, ~NE-SW  
 267 and ~WSW – ENE trending strike-slip faults with a gently prevailing right-lateral kinematic pattern were identified  
 268 across the studied area (Fig. 2,5b). In spatial context of large volcanic centres (e.g. Wobitcha, Duguna Fango and  
 269 Awassa Caldera; Fig. 2) the caldera-related ring faults were found having a curved asymmetric shape, mostly  
 270 parallel to the caldera rim. These faults predominantly dip steeply to moderately inward to the centre of the caldera.  
 271 Extensional joints occur in three distinct sets with a ~ N – S, NNE – SSW and E (WNW) – W (ESE) trend (Fig. 5c).



272  
 273 Fig. 4. (a) Simplified geological map of the southern part of the Main Ethiopian Rift (Hossana and Dilla areas); (b)  
 274 Schematic stratigraphic chart of the Main Ethiopian Rift (Dilla and Hossana areas). Compiled using unpublished  
 275 geological maps 1:250 000 Geological Survey of Ethiopia.  
 276



277



278

279

280

281

Fig. 5. Field structural measurements of faults (equal area projection to lower hemisphere) and extensional joints (rose diagram) from the southern part of the Main Ethiopian Rift (Hossana and Dilla areas).



282

283

284

285

286

287

288

289

290

#### 4.3. Slope instabilities

291

292

293

294

295

Active extensional tectonics and the intense volcanism associated with the East African Rift System (e.g. Agostini et al., 2011; Chorowicz, 2005) represent one of the main reasons for frequent hazardous geological phenomena in the Main Ethiopian Rift (MER). Characteristic rift-related morphology, seasonal climatic conditions and inappropriate human interference in the landscape create suitable conditions for hazardous geological processes. Endogenous risk factors such as earthquakes, volcanism and post-volcanic phenomena are closely related with tectonics in this area.



296 The geomorphology is highly variable across the MER and is mainly the result of volcanic and tectonic events with  
297 the associated erosional and depositional processes (Billi, 2015). The principal feature of the MER is the graben  
298 bounded by normal faults. The drainage network is largely controlled by tectonic activity and lithological variation.  
299 Parts of grabens form endorheic depressions filled by temporal lakes. The area is climatically highly variable; the  
300 average amounts of annual rainfall vary from 500 in the Gibe and Omo Gorges to 2,600 mm on the escarpments and  
301 the adjacent highlands. The mean annual temperature is about 20°C.  
302 Slope failures, erosion, floods and the occurrence of ground fissures are the most common geological hazard  
303 investigated in the Hossana and Dilla areas. Landslides, debris flows and rockfalls represent common exogenous  
304 hazards distributed mainly on the fault scarps (Fig. 2 and 7 a). The subsidence of the rift floor and consequent uplift  
305 of the highland lead to isostatic disequilibrium resulting in intensive head-ward erosion and slope processes. Most of  
306 the slope instabilities represent deep seated complex fossil failures (Fig. 7 b) that host reactivated smaller landslides  
307 and debris flows which are triggered by adverse anthropogenic practices (road construction, deforestation,  
308 overgrazing) or river undercutting (fig. 7 e, f).  
309 Rare lateral spread, with typical horst and graben features at the head, and many secondary shear surfaces have been  
310 encountered in the complex un-welded ignimbrites and unconsolidated pyroclastic deposits with horizons of  
311 paleosoils following the slip zone of this landslide (fig. 7 c). Topographic depressions with a higher degree of  
312 saturation are often noted to have the long run effect of triggering landslides and debris flow on the slopes below  
313 them (fig. 7 d, f).  
314



315  
316 *Fig. 7. Field photographs of various types of geohazards in MER – Hossana and Dilla areas. (a) Toppling and*  
317 *subsequent rock fall of welded ignimbrites in the crown of a deep-seated landslide situated close to a fault scarp in*  
318 *the western highland area (Dilla area; NW of Arba Minch town). (b) Large landslide in Dilla area (5 km SW of*  
319 *Mejo town). (c) Tilted blocks of deep-seated landslide southwest to Awassa. (d) Undrained depression in the deep-*  
320 *seated fossil landslide east of Dilla Town. (e) Tension cracks in the crown of a shallow landslide reactivated by road*  
321 *construction, west of Arba Minch. (f) Recent debris flow accumulation below road construction in the landslide area*  
322 *west of Mejo.*

323  
324  
325  
326  
327  
328  
329

#### 4.4. Statistical analysis

Statistical analysis was carried out to better understand the influence of various surface processes and conditions (precipitation, vegetation, slope, land cover) and geological parameters (rock mass strength, proximity of faults, lineaments) on the formation of landslides and rockfalls. However, anthropogenic factors could not be evaluated statistically because the relevant data are not available.



330 **4.4.1. Descriptive statistics**

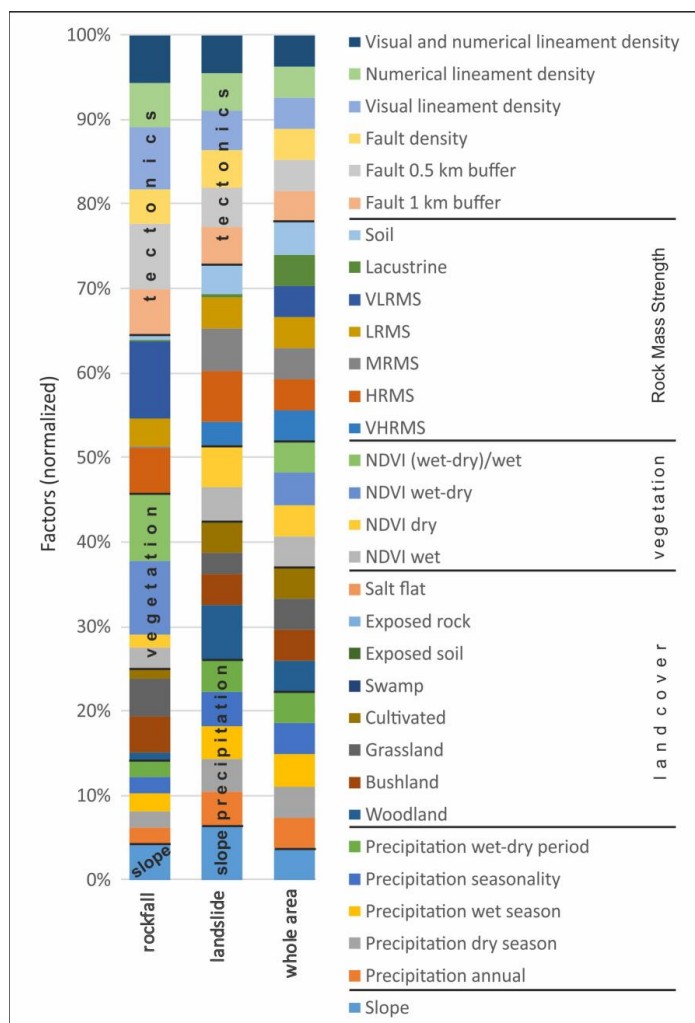
331 For the purposes of descriptive statistics, Rock Mass Strength (RMS) was coded as follows: Very High RMS = 7,  
 332 High RMS = 6, Medium RMS = 5, Low RMS = 4, Very Low RMS = 3, Soils = 2, Lacustrine deposits = 1. A  
 333 significant correlation between RMS and slope and most precipitation parameters was found (see Table 1). More  
 334 wet and seasonal areas occur on steeper slopes formed by stronger (less weathered) rocks. Most of the steep slopes  
 335 in the study area are active normal fault escarpments. Another interesting statistically significant correlation is  
 336 shown by Slope and most of the precipitation parameters and the vegetation index (NDVI) of the dry period. Steeper  
 337 slopes and higher altitudes are probably attracting clouds and precipitation, while flat lowlands allow clouds to pass  
 338 by without precipitation. Significant correlations can also be found within various precipitation parameters, within  
 339 selected vegetation parameters and also between these two groups (precipitation and vegetation), which was  
 340 supposed. No significant correlation was found between the proximity of faults and lineaments (expressed by faults  
 341 and lineaments density) and other parameters. It seems to be an independent variable very suitable for geostatistical  
 342 evaluation.  
 343

	RMS	Slope	Precipitation				NDVI			Faults and lineaments density	
			Annual	Dry period	Wet period	Seasonality	Wet-dry period	Wet period	Dry period		Wet-dry period
RMS	1.00	<b>0.44</b>	<b>0.49</b>	0.17	<b>0.43</b>	<b>0.58</b>	<b>0.39</b>	0.10	0.07	-0.01	0.13
Slope	0.44	1.00	<b>0.37</b>	0.11	<b>0.25</b>	<b>0.37</b>	<b>0.22</b>	0.16	<b>0.24</b>	-0.12	-0.11
Precipitation annual	0.49	0.37	1.00	<b>0.61</b>	<b>0.47</b>	<b>0.73</b>	<b>0.35</b>	<b>0.28</b>	<b>0.37</b>	-0.16	-0.14
Precipitation dry period	0.17	0.11	0.61	1.00	-0.11	-0.01	<b>-0.27</b>	0.14	<b>0.41</b>	<b>-0.29</b>	-0.18
Precipitation wet period	0.43	0.25	0.47	-0.11	1.00	<b>0.80</b>	<b>0.99</b>	0.15	<b>-0.39</b>	<b>0.44</b>	0.06
Precipitation seasonality	0.58	0.37	0.73	-0.01	0.80	1.00	<b>0.77</b>	<b>0.20</b>	0.06	0.07	0.03
Precipitation wet-dry period	0.39	0.22	0.35	-0.27	0.99	0.77	1.00	0.12	<b>-0.44</b>	<b>0.47</b>	0.09
NDVI wet period	0.10	0.16	0.28	0.14	0.15	0.20	0.12	1.00	0.16	<b>0.46</b>	-0.05
NDVI dry period	0.07	0.24	0.37	0.41	-0.39	0.06	-0.44	0.16	1.00	<b>-0.80</b>	-0.10
NDVI wet-dry period	-0.01	-0.12	-0.16	-0.29	0.44	0.07	0.47	0.46	-0.80	1.00	0.06
Faults and lineaments density	0.13	-0.11	-0.14	-0.18	0.06	0.03	0.09	-0.05	-0.10	0.06	1.00

344 *Table 1. Correlation matrix of the selected factors controlling distribution of geohazards in the MER area. Number*  
 345 *of samples 153, critical value for correlation coefficient (R) at the 95 % significance level is 0.195. A statistically*  
 346 *significant (95 %) R is in bold.*  
 347  
 348

349 **4.4.2. Geostatistics**

350 The mean values of various geological, tectonic, climatic, vegetation and land use factors were calculated for each  
 351 landslide polygon area. The normalized difference vegetation index (NDVI) is adopted from MODIS images of  
 352 2016 while density of lineaments is expressed as \*[E+06]. The Kernel Density tool of the Spatial Analyst  
 353 Tools/Density (ArcGIS 10.6) was used for evaluating the faults and lineaments density in MER on a scale of 1:250  
 354 000 (see Table 2). Proximity to tectonic features is expressed in terms of the percentage area of a particular  
 355 geohazard within a particular buffer zone (500 m and 1 km buffer).  
 356



357  
 358  
 359  
 360  
 361  
 362  
 363  
 364  
 365  
 366  
 367  
 368  
 369  
 370  
 371  
 372

Fig. 8. Plot of mean values of particular factors occurring across landslides and rockfalls polygons normalized to the mean value for the whole area. Diagram shows the relative importance of each factor in comparison with the whole set of factors.

Most landslides and rockfalls form on steeper slopes close to faults and in areas with higher lineament density. Rockfalls are formed on steeper slopes than landslides (Table 2) but slope factor has higher importance for the formation of landslides (in comparison to other factors, see Fig. 8). Rockfalls typically occur in areas receiving lower precipitation. Most of them occupy areas with grassland and, to a lesser extent, also on cultivated land and bush land cover. Higher vegetation seasonality is also found to coincide well with rockfall occurrences. A low, very low and high rock mass strength class probably influence the occurrence of rockfalls (see Table 2 and Fig. 8). While landslides are formed in areas with higher precipitation and higher precipitation seasonality. Woodland, bushland, grassland and cultivated areas with higher vegetation density and low vegetation seasonality are found to have an affinity with landslide occurrences. All range of rock mass strength classes (low, medium and high) occur in areas of landslides.



geohazard\factor	Slope (degree)	Precipitation		P. seasonality		Vegetation		V. seasonality		Rock Mass Strength					Tectonics		Lineaments density			Landuse										
		annual [mm]	Dec-Jan (Dry) [mm]	Jul-Aug (Wet) [mm]	monthly Jr	wet-dry [mm]	NDVI/wet(Aug)	NDVI/dry (Jan)	NDVI/Aug-Jan	(Aug-Jan)/Aug [%]	VHRMS [%]	HRMS [%]	MRMS [%]	LRMS [%]	VL RMS [%]	Lacustrine [%]	Soil [%]	within 1 km buffer	within 0.5 km buffer	faults	visual	numerical	vis and num	woodland [%]	bushland [%]	grassland [%]	cultivate [%]	swamp [%]	exposed soil [%]	water [%]
rockfall	<b>17.2</b>	1041	44	312	54	268	<b>5412</b>	<i>3149</i>	<b>2263</b>	42	0	<b>27</b>	3	<b>40</b>	<b>25</b>	1	3	<b>88</b>	<b>66</b>	<b>155</b>	<b>341</b>	<b>227</b>	<b>227</b>	8	<b>18</b>	<b>48</b>	<b>21</b>	1	0	4
landslide	<b>15.6</b>	<b>1248</b>	<b>51</b>	<b>351</b>	<b>66</b>	<b>300</b>	<b>5296</b>	<b>5510</b>	-214	-4	4	<b>18</b>	<b>38</b>	<b>26</b>	0	1	12	43	24	<b>97</b>	<b>131</b>	<b>111</b>	<b>108</b>	<b>38</b>	9	<b>16</b>	<b>37</b>	0	0	0
whole area	9.0	1172	48	333	61	285	4868	4297	571	12	5	11	28	26	6	11	13	36	19	82	103	95	88	22	9	24	36	1	1	6

373  
 374 *Table 2. Mean values for each geohazard polygon area compared to the whole area of Hossana and Dilla. NDVI*  
 375 *calculated from Modis images 2016, lineaments density is \*[E+06]. The proximity of tectonics is expressed in the*  
 376 *percentage area of the particular geohazard within the buffer. **Bold underline** - highly above average; **bold** - above*  
 377 *average; italics - below average.*

#### 379 4.5. Case studies – Mejo and Arba Minch areas

380 Two areas with contrasting lithological, tectonic, climatic and vegetation settings and a similar size and morphology  
 381 of landslides and rockfalls were selected for a detailed study. The study areas correspond with 1:50 000 map sheets  
 382 (for location see Fig. 2).

##### 384 4.5.1. Mejo Site

385 The Mejo study area is located 60 km east of the main rift valley on the upland plateau of the south-eastern flank of  
 386 the MER. The Gambelto and Genale rivers drain the area southeast to Somalia form a typical morphology with  
 387 deeply incised N-S trending valleys in the central part and volcanic plateaus along the south-western and eastern  
 388 margin (Fig. 9). These volcanic plateaus attain an elevation slightly above 2000 m asl at east and around 2,100 m asl  
 389 at south-west. Neoproterozoic medium-grade metamorphic rocks crop out mainly in the deeper part of the valleys  
 390 below the altitude of ca 1900 m and the deepest parts reach below 1000 m asl. Thus, the area has a prominent  
 391 topography with an altitude difference of more than 1000 m; the average slope in the area is more than 14 degrees.  
 392 The overlying volcanic deposits are of Eocene to Pleistocene age (Verner et al., 2018a; Verner et al., 2018b). The  
 393 local climate is humid, the annual precipitation is ~1,200 mm to ~1,550 mm (average 1393 mm) and highly  
 394 seasonal usually with two peaks corresponding to April-May and August-October with more than 125 mm monthly  
 395 average rainfall, while the rest of the months have a monthly average rainfall of slightly more than 40 mm. The  
 396 difference between the average wet (July + August) and dry season (December + January) is 310 mm (CDE, 1999).  
 397 Vegetation cover is dense (NDVI values almost double comparing the Arba Minch area) and moderately seasonal  
 398 (see Table 3). Due to intense weathering the area is dominated by rocks with low and medium mass strengths. The  
 399 dominant land cover is woodland and bushland, cultivated areas form up to 25 % of the area.

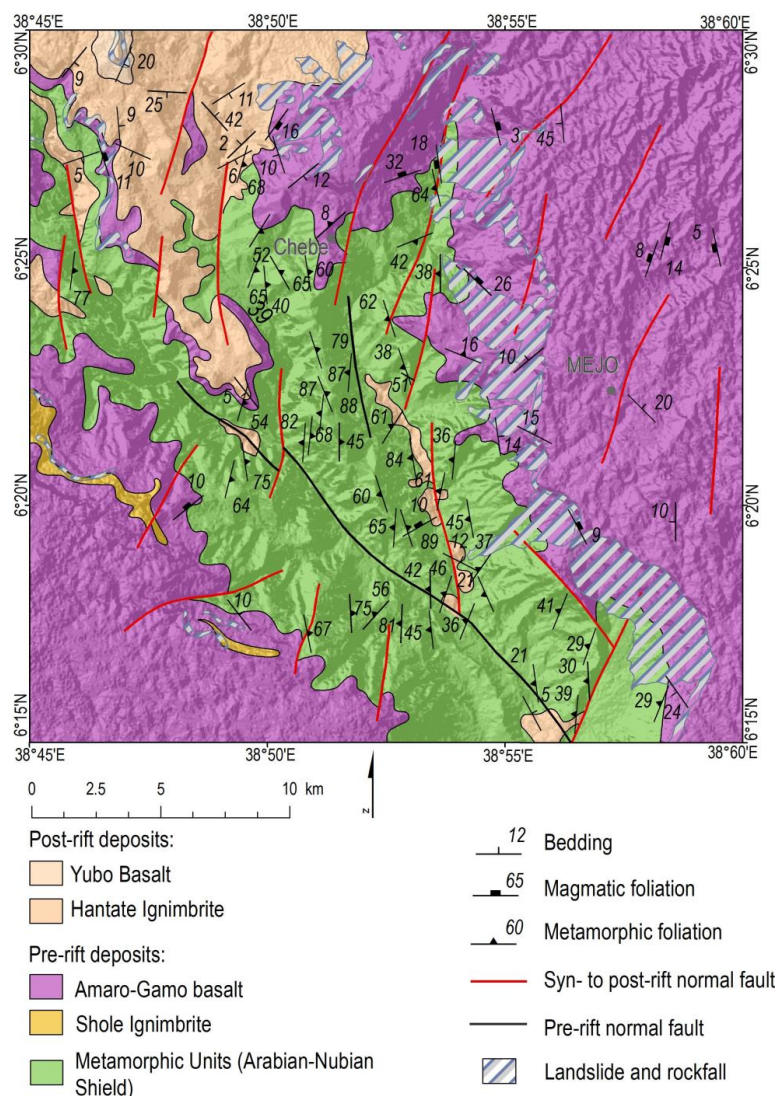
400 The area is formed by two units: (i) Metamorphic basement consisting of foliated biotite orthogneiss with minor  
 401 lenses of amphibolites outcropped in the lower parts of the slope and the bottom of valleys. The orthogneiss is  
 402 moderately to strongly weathered, the lenses of amphibolites have higher intact strength with a lower degree of  
 403 weathering. The foliation of metamorphic rocks is often oriented downslope, parallel with the topography of the  
 404 instable slopes. (ii) The volcanic complex overlying the metamorphic basement is formed by a roughly 500 metre  
 405 thick succession of basalt and trachybasalt massive lava flows and intercalations of palaeosols, fine basaltic scoria  
 406 layers and epiclastic deposits up to 2 m thick. The lava flows are moderately to strongly weathered with high  
 407 fissured permeability, the pyroclastic layers, paleosols and strongly weathered horizons with high content of clay  
 408 minerals may form semi-horizontal barriers for water movement resulting in higher plasticity and a reduction of  
 409 permeability (Verner et al., 2018a; Verner et al., 2018b).

410 Most of the fault structures were identified in the complex of metamorphic rocks, without evidence of young  
 411 reactivation. The youngest faults and fault zones belonging to the East African Rift System are rare and have no  
 412 significant effect on the overall tectonic pattern of the area. These minor faults dip steeply to ~E or ~W, bearing  
 413 well-developed steeply plunging slickensides and normal kinematics. The minor subordinate set of normal faults  
 414 have a ~ W (WNW) to E (ESE) trend. The fault displacement is relatively low across the area, reaching a maximum  
 415 of 100 metres in the vertical section (Verner et al., 2018a; Verner et al., 2018b). The prominent morphology, with up  
 416 to 1000 m deeply incised valleys, is made almost solely by erosion caused by Neogene uplift.

417 A large and deep-seated complex landslide area occurs in the slope of the eastern banks of the Gambelto Valley. The  
 418 landslide areas vary in length from several hundred metres to 4 kilometres, with a width of up to 2 kilometres (see  
 419 Fig. 9). The landslide complexes are characterized by amphitheatre (horse-shoe)-shaped edges of the main scarps  
 420 and reach up to 200 metres high, and 50 to 100 metre high minor scarps. Commonly, tilted blocks, endorheic



421 depressions and a number of springs have also been noted in the landslide zone. Reactivated parts are characterized  
 422 by small-scale (tens to hundreds of metres) and shallow-seated debris flows, slumps and rock-falls accompanied by  
 423 the subsidence of surface, cracks or curved tree trunks, which were observed close to the new road construction.  
 424 Most landslides are fossil and inactive. The preservation of colluvial deposits is limited, while in the depressed  
 425 domain and the arched accumulation area of the landslide they are covered by boulders and blocks. The morphology  
 426 of the main and minor scarps is relatively sharp and the accumulation zone is strongly modified by erosional  
 427 processes with a smooth and undulating topography, an absence of a hummocky landscape and traverse ridges. Most  
 428 of the reactivated parts are represented by small-scale and shallow-seated failures triggered by the poor design of  
 429 local road construction.  
 430



431  
 432 *Fig. 9. Geological and tectonic map of the Mejo Site with landslides and rockfalls indicated. For location, see Fig.*  
 433 *2.*  
 434





435 The mean values of the same factors as for the Hossana and Dilla areas (see section 4.4.2) were also calculated for  
 436 each landslide and rockfall polygon area in the case of the Mejo site. The same calculations and symbology as in  
 437 Table 2 was used for most parameters, but faults and lineaments data were adopted from more detailed studies at a  
 438 scale of 1:50 000 (Verner et al., 2018a; Verner et al., 2018b; Verner et al., 2018c; Verner et al., 2018d) and the faults  
 439 and lineaments density is calculated by a Line Density tool (ArcGIS 10.6. Spatial Analyst Tools) and expressed as  
 440  $*[E+02]$ . Here the landslides and debris-flows are situated in areas with much higher slopes, compared to the overall  
 441 study area (see Fig. 10 and Table 3). They are also formed in areas with a higher vegetation density and medium and  
 442 low RMS. Landslide and debris-flow areas have a much higher density of lineaments. They are also dominantly  
 443 vegetated by woodlands, cultivated areas are a minor land cover.  
 444

445  
 446  
 447  
 448

geohazard\factor		Precipitation			P. seasonality		Vegetation		V. seasonality		Rock Mass Strength				Tectonics			Landuse							
		Slope [degree]	annual [mm]	Dec-Jan (Dry) [mm]	Jul-Aug (Wet) [mm]	monthly 1s	wet-dry [mm]	NDVI wet (Aug)	NDVI dry (Jan)	NDVI Aug-Jan	(Aug-Jan)/Aug [%]	VHRMS [%]	HRMS [%]	MRMS [%]	LRMS [%]	Lacustrine [%]	1 km buffer [%]	0.5 km buffer [%]	faults density	lineaments density	woodland [%]	bushland [%]	grassland [%]	cultivated [%]	water [%]
Mejo	landslide and debris-flow	17.6	1335	46	346	75	300	6303	7278	-975	-0.15	2.06		31.7	60.8	5.4	50.9	27	33.8	58	72	3			26
	whole area	14.2	1393	47	357	78	310	5548	6421	-874	-0.16	7.89		28.3	41.9	22	61.5	36	33.6	34	53	19	3.1	24.8	
Arba	landslide and rockfall	14.9	1070	60	188	45	128	5361	6412	-1051	-0.20			42.7	56.7	0.6	97.1	68	67.0	78		30		70	
Minch	whole area	9.8	1068	59	189	46	130	3051	3909	-858	-0.28	3.01		21.2	49.5	26	68.8	44	43.6	51	1.14	19.2		51.2	28.4

Table 3. Mean values for each geohazard polygon area compared to the overall area of Mejo and Arba Minch respectively.

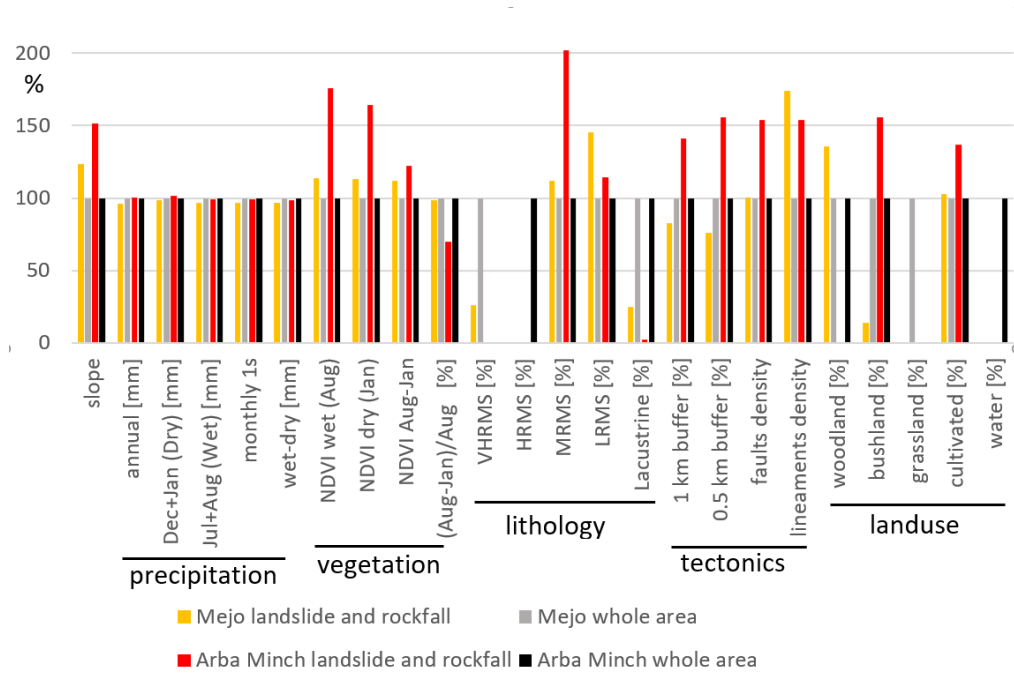


Fig. 10. Plot of mean values of particular factors occurring across merged polygons of landslides and rockfalls normalized to the mean value for the overall area. Mejo and Arba Minch sites evaluated separately.

#### 4.5.2. Arba Minch Site

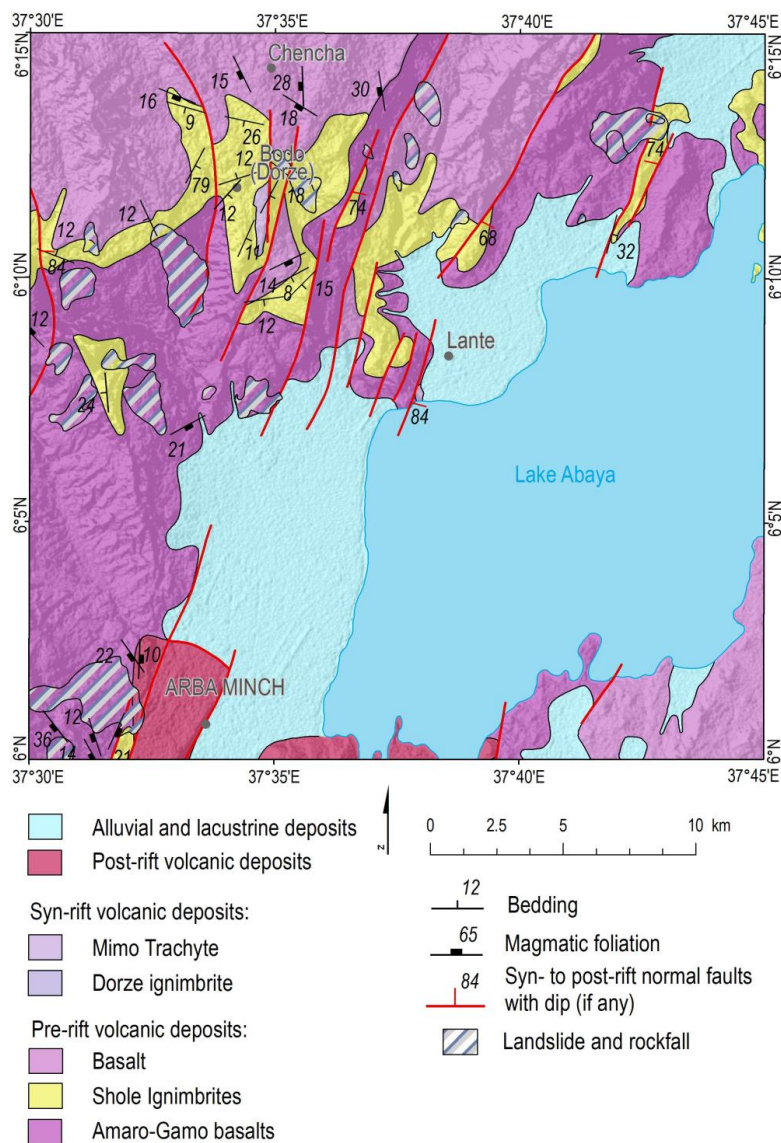
The Arba Minch study area is located directly in the main rift valley on the western normal fault escarpment. The total displacement of the syn- and post-rift normal faults is more than 1500 metres. The average slope in the area is less than 10 degrees because a large part of the area is covered by Abaya Lake (see Fig. 11). The area is less humid, compared to Mejo, with an average annual precipitation of 1068 mm and precipitation is moderately seasonal, the difference between the wet and dry season is 130 mm. But significant variations in precipitation have been recorded



459 in apical parts of mountain ridges, such as Chench, attaining, on average, an altitude of 2,700 m asl with 1,390 mm  
460 of rainfall, whereas in the low-lying plains with an average elevation of about 1,200 m asl around the city of Arba  
461 Minch the precipitation fluctuates around 780 mm (CDE, 1999). Vegetation cover is moderate (NDVI values almost  
462 half of Arba Minch area) and moderately seasonal (see Table 3). Rocks with low and medium mass strengths and  
463 lacustrine deposits dominate the area. The dominant land cover type is cultivated areas (form up to 51 %), bushland  
464 and water surface are also abundant types. The area is formed by lower Eocene to Pleistocene volcanic and  
465 volcanoclastic rocks, which are a product of episodic eruptions. They mostly have a bimodal composition with  
466 alternating basic volcanic rocks and acidic pyroclastic rock intercalations (Verner et al., 2018 c; Verner et al.,  
467 2018d). The prevailing faults are mostly parallel to the axis of the MER forming the area's prominent morphological  
468 features. These major normal faults dip steeply to ESE or SE, trending NNE–SSE. Moreover, subordinate normal  
469 faults were identified, predominantly steeply inclined faults trending WNW–ESE, which are perpendicular to the  
470 prevailing rift-parallel normal faults. Fault displacement is relatively high across the area, reaching a minimum of  
471 1,000 metres forming prominent morphology with an altitude difference of up to 1,500 m between the plateau and  
472 graben floor.

473 The slope failures are located in the western steep fault scarps separating the bottom of the rift valley with Abaya  
474 Lake representing a local erosional base at an elevation of 1,200 m asl and the western highland with an undulating  
475 landscape at an elevation of between 2,000 and 2,400 m asl. The scarps are often modified by deep-seated slope  
476 failures. The lower parts of the slopes form moderately weathered basalts and trachybasalt with minor pyroclastic  
477 fall layers of volcanic ash reaching up to 2 m in thickness and a reddish paleosol up to 30 cm thick. The ridges and  
478 upper parts are formed of welded ignimbrites with minor rhyolitic ash fall deposits and paleosol horizons. Volcanic  
479 rocks are variably affected by intense fracturing, jointing and mega tectonic fault systems. Basalts and trachybasalts  
480 are with a higher degree of weathering, while the welded ignimbrites with common columnar jointing are more  
481 resistant. The volcanic units have fissured permeability. Mainly the ignimbrites represent rocks with high  
482 permeability, on the other hand the highly weathered basalt, the intercalation of fine grained pyroclastics and  
483 paleosol horizons could form hydrogeological horizontal barriers because of the high content of clay minerals. Most  
484 of the landslides are represented by deep-seated complex slope deformations including toppling, rock-fall, rockslide,  
485 rotational landslides and debris flows. These slope failures appear to be currently stable; the morphology is modified  
486 by subsequent exogenous processes as in the Mejo area. Only several small-scale active landslides triggered by river  
487 erosion and human intervention were observed.

488



489  
 490 *Fig. 11. Geological and tectonic map of Arba Minch Site with landslides and rockfalls indicated. For location, see*  
 491 *Fig. 2.*  
 492

493 The mean values of the same factors as for the Mejo site were also calculated for each landslide and rockfall  
 494 polygon area at the Arba Minch site. Here the landslides and rockfalls are situated in areas with much higher slopes,  
 495 compared to the overall study area (see Fig. 10 and Table 3), there is a much higher density of faults and lineaments  
 496 close to faults. They are also formed in areas with much higher vegetation density and medium and low RMS.  
 497 Landslide and rockfall areas are also dominantly covered by cultivated areas with woodlands taking a minor role.  
 498



## 499 5. Discussion

### 500 5.1. Main Ethiopian Rift (Hossana and Dilla area)

501 The progressive changes of the paleo-stress regime during the active continental extension and faulting in the MERS  
502 (e.g. Corti et al. 2018; Zwaan and Schreurs, 2020) increase the tectonic anisotropy of rocks, slope instabilities along  
503 major and subordinate fault escarpments which have a pronounced effect on the genesis and formation of landslides.  
504 Several tectonic models explain the kinematics and paleostress conditions of the regional extension / transtension  
505 from the beginning of the rifting (ca 12 Ma) to the present (for the review see Zwaan and Schreurs, 2020). Some  
506 models suppose continuous a NW – SE oriented extension (e.g. Chorowicz, 2005) in the early phase which later  
507 changed to its current E-W direction (Bonini et al., 2005; Wolfenden et al., 2004). Alternatively, other models also  
508 assume a permanent E – W to ESE – WNW oriented extension (e.g. Agostini et al., 2009; Erbello and Kidane,  
509 2018).

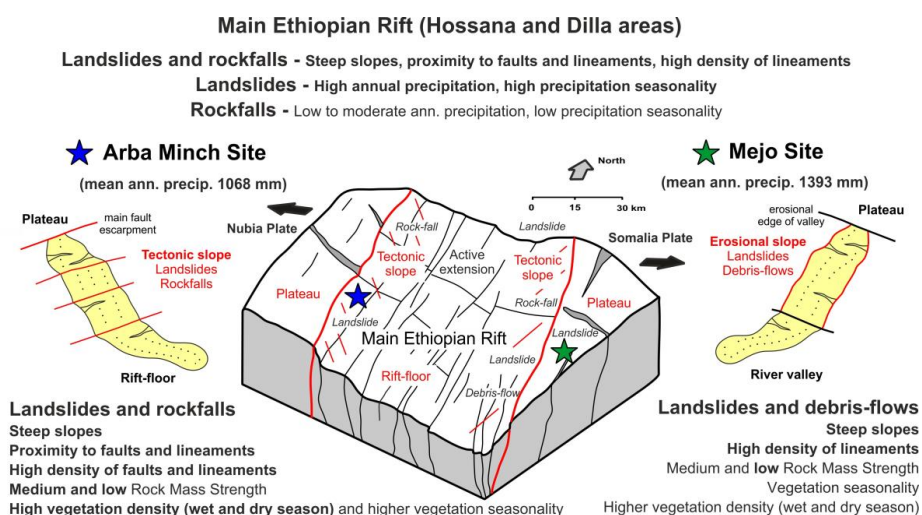
510 Proximity to faults and lineaments have strong influence on the occurrence of rock falls and landslides in  
511 tectonically active areas worldwide (e.g. Chang et al, 2018; Kumar et al., 2019 and references therein). In the MER,  
512 both rockfalls and landslides typically occur on areas with steep slope, close to faults and with higher density of  
513 faults and lineaments. The latter parameter also reflects faults and fracture zone intersections and, according to  
514 geostatistic evaluation (Table 2), is more important for the formation of rockfalls than landslides. Rockfalls also  
515 show a much higher affinity to the proximity of faults.

516 Rockfalls occur in areas with lower precipitation, while for landslides high precipitation and high precipitation  
517 seasonality is typical. It correlates well with high vegetation density and low vegetation seasonality, which are found  
518 to have strong affinity with landslide occurrences. Thus, precipitation does not seem to be an important factor for  
519 rockfall formation but is important for landslides.

520 Rockfalls and landslides occur on areas with bushland, grassland and cultivated landcover. It leaves deforestation as  
521 one of the possible triggering factors. They also occur in areas with a wide range of rock mass strength classes (very  
522 low, low, medium and high) so lithology and intensity of weathering do not seem to be an important triggering  
523 factor.

524 In the large area of the MER the vast majority of slope instabilities is located on active normal fault escarpments  
525 (Fig. 12). This is a major natural triggering factor for rockfalls. While for landslides there is also the important  
526 influence of higher precipitation, precipitation seasonality and vegetation density and seasonality.

527



528 Fig. 12. Sketch diagram summarising the main factors controlling the formation and distribution of particular slope  
529 failures in the MER and in the Arba Minch and Mejo study sites.  
530

531

### 532 5.2. Arba Minch case study

533 Slope instabilities, mostly landslides and rockfalls, here are situated in areas with much steeper slopes, a much  
534 higher density of faults and lineaments and close to major faults. The majority of the large-scale slope instabilities of  
535 this area is strongly associated with active tectonic morphological features characterized by straight fault scarps with  
536 triangular facets, large downthrown blocks, parallel sets of erosional valleys and asymmetrical ridges with SSW-



537 NNE trending. These features are associated with active normal faults having large displacements (total vertical  
538 displacement of the western rift escarpment is more than 1500 m). Slope instabilities are also formed in areas with a  
539 much higher vegetation density and medium and low RMS. Volcanic rocks are variably affected by intense  
540 fracturing along faults, these zones are often altered, which lowers the slope stability of the rock environment.  
541 Alteration is also enhanced by more intense water-rock interactions – most springs are located on fault zones (Arba  
542 Minch means “Forty Springs”). Precipitation was not confirmed as an important factor.  
543 The Arba Minch area is seismically active, according to the catalogue of earthquakes of the United States  
544 Geological Survey (USGS) several earthquakes have been documented around Abaya Lake since 1973 with  
545 magnitudes between 4 and 6 (USGS, Earthquake Hazards Program, 2017). This active tectonic is also documented  
546 by young faults affecting Quaternary volcanic rocks and sediments outcropped around the town of Arba Minch  
547 (Verner et al., 2018 c, d).

### 549 5.3. Mejo case study

550 Landslides and debris-flows here are situated in areas with steep slopes. The geomorphology of the area is almost  
551 unaffected by rift tectonics; evidence of young faulting as displacement of the Pleistocene and Holocene rocks,  
552 straight fault scarps with triangular facets, has not been observed. The steep slopes are formed and strongly modified  
553 by intensive head-ward erosion. The incision of the valley as a result of a lowered erosional level and highland uplift  
554 could be the driving factor for the slope instability in the case of the Mejo area. Geomorphic proxies and the  
555 thickness of flood basalts suggest that the more tectonically active south-eastern escarpment of the CMER and  
556 SMER (where the Mejo site is situated) are experiencing a relatively higher rate of tectonic uplift compared to the  
557 south-eastern escarpment of the northern MER and the Afar Depression (Xue et al., 2018; Sembroni et al., 2016).  
558 This can also be noted from the Eocene-Oligomiocene basalts base (35 – 26 My) occurring in Arba Minch at an  
559 elevation of around 1050 m asl compared to their occurrence at a much higher elevation in Mejo, at around 1900 m  
560 asl (Verner et al., 2018a; Verner et al., 2018b; Verner et al., 2018c; Verner et al., 2018d).  
561 Another factor causing the decrease of slope stability could be local lithological properties (dominance of medium  
562 and low RMS characteristic for slope instabilities in the area): (i) frequent intercalations of palaeosols with a high  
563 content of clay minerals and low permeability, (ii) a strongly weathered metamorphic basement with foliation often  
564 concordant with the landscape forming a very weak lithological environment, which is favourable for slope  
565 processes. No young volcanic features and products have been observed; the probability of earthquakes related to  
566 volcanic eruptions is very low in the Mejo area, where the nearest earthquakes were recorded 60 km NW of the  
567 study area.

### 569 5.4. Comparison of Arba Minch and Mejo sites

570 Landslides at both sites are similar from the geomorphological point of view, i.e. old, stabilized, smoothed by  
571 erosion. Young reactivations are very localized and mostly due to human activity. Both study areas have seasonal  
572 humid climates with a prominent summer (mid June – mid September) rain season, but the Mejo study area, which  
573 is situated 90 km east of Arba Minch, 60 km out of the main rift valley on the fast-uplifting plateau, is more humid.  
574 In the Mejo area the mean annual rainfall is 30 % higher (1393 mm) compared to Arba Minch (1068 mm), most of  
575 the precipitation difference falls in the rainy season, while during the dry months the precipitation at both localities  
576 is comparable (Table 3).  
577 Steep slopes associated with active faulting and hydrogeological conditions favouring rock alterations along these  
578 zones are probably the main factors triggering the formation of slope instabilities in Arba Minch. In addition to these  
579 factors, seismic events could also be speculated as one of the triggering factors.  
580 The combination of a deeply weathered Proterozoic basement and steep slopes formed by intense head-ward  
581 erosional processes due to rapid uplift could represent the main factors for creating favourable conditions for  
582 landslide evolution in Mejo (Fig. 12). More intense precipitation may also contribute to slope instability.

### 584 6. Conclusions

585 Active continental rifting has a distinct effect on the formation of landslides. The formation, superposition, and  
586 polyphase reactivation of fault structures in the changing regional stress-field increase the tectonic anisotropy of  
587 rocks and increase the risk of slope instabilities forming. The new structural data from the CMER and SMER  
588 support a model of progressive change in the orientation of the regional extension from NW – SE to the recent  
589 E(ENE) – W(WSW) direction driven by the African and Somalian plates moving apart with the presumable  
590 contribution of the NNE(NE) – SSW(SE) extension controlled by the Arabic Plate.



591 An evaluation at the regional scale of the central and southern MER demonstrates that slope instabilities, mainly  
592 landslides and rockfalls, occur on steep slopes, which are almost exclusively formed on active normal fault  
593 escarpments. Landslides are also importantly influenced by higher annual precipitation, higher precipitation  
594 seasonality and vegetation density and seasonality, while rockfalls have an affinity to vegetation seasonality only.  
595 Different geological, geomorphological, and climatic conditions can lead to formation of similar types of slope  
596 instabilities. A detailed study on active rift escarpment in the Arba Minch area revealed similar affinities as in the  
597 regional study of MER. Slope instabilities here are closely associated with steep, mostly faulted, slopes and a higher  
598 density of vegetation. Active tectonics and probably also seismicity are the main triggers. While the detailed study  
599 situated in the Mejo area on the uplifting Ethiopian Plateau 60 km east of the rift valley show that the occurrence of  
600 slope instabilities is strongly influenced by steep erosional slopes and deeply weathered Proterozoic metamorphic  
601 basement. Landslides here are often formed in areas densely fractured and with foliation concordant with  
602 topography. Rapid head-ward erosion, unfavourable lithological conditions and more intense precipitation and  
603 higher precipitation seasonality are the main triggers.

604

605 *Competing interests.* The authors declare that they have no conflict of interest.

606

607 *Acknowledgements.* The research was funded by the Czech Development Agency in the framework of development  
608 project No. 281226/2018-ČRA “Implementation of a Methodical Approach in Geological Sciences to Enhance the  
609 Quality of Doctoral Studies at the Addis Ababa University (Ethiopia)” (to K. Verner) and project No. 280614/2019-  
610 ČRA “Ensuring Sustainable Land Management in Selected Areas of Ethiopia on the Basis of Geoscientific  
611 Mapping” (to K. Verner). We thank our many colleagues from the Geological Survey of Ethiopia and Addis Ababa  
612 University (School of Earth Sciences) for their help in the acquisition, processing and interpretation of the data,  
613 especially to Aberash Mosisa and Wubayehu Dessalegn Sallile. Many thanks to Richard Withers for the English  
614 proof reading.

615

616

## 617 **References**

618

- 619 Abate, M., Nyssen, J., Steenhuis, T. S., Moges, M. M., Tilahun, S. A., Enku, T., and Adgo, E.: Morphological  
620 changes of Gumara River channel over 50 years, upper Blue Nile basin, Ethiopia, *Journal of Hydrology*,  
621 255, 152-164, <https://doi.org/10.1016/j.jhydrol.2015.03.044>, 2015.
- 622 Abebe, T., Manetti, P., Bonini, M., Corti, G., Innocenti, F., Mazzarini, F., and Pecsckay, Z.: Geological map (scale  
623 1:200 000) of the northern main Ethiopian rift and its implication for the volcano-tectonic evolution of the  
624 rift, *Geological Society of America, Boulder, Colorado, Maps and Charts series, MCH094*, 2005.
- 625 Abebe, B., Dramis, F., Fubelli, G., Umer, M., and Asrat, A.: Landslides in the Ethiopian highlands and the Rift  
626 margins, *Journal of African Earth Sciences*, 56, 131-138, <https://doi.org/10.1016/j.jafrearsci.2009.06.006>,  
627 2010.
- 628 Acocella, V.: Coupling volcanism and tectonics along divergent plate boundaries: Collapsed rifts from central Afar,  
629 Ethiopia, *Geological Society of America Bulletin*, 122, 1717–1728, <https://doi.org/10.1130/B30105.1>,  
630 2010.
- 631 Agostini, A., Corti, G., Zeoli, A., and Mulugeta, G.: Evolution, pattern, and partitioning of deformation during  
632 oblique continental rifting: Inferences from lithospheric-scale centrifuge models, *Geochemistry*,  
633 *Geophysics, Geosystems*, 10, 1-11, <https://doi.org/10.1029/2009GC002676>, 2009.
- 634 Agostini, A., Bonini, M., Corti, G., Sani, F., and Manetti, P.: Distribution of Quaternary deformation in the central  
635 Main Ethiopian Rift, East Africa, *Tectonics*, 30, <https://doi.org/10.1029/2010TC002833>, 2011.
- 636 Altin, T. B. and Altin, B. N.: Development and morphometry of drainage network in volcanic terrain, Central  
637 Anatolia, Turkey, *Geomorphology*, 125, 485–503, <https://doi.org/10.1016/j.geomorph.2010.09.023>, 2011.
- 638 Asfaw, L. M.: Development of earthquake-induced fissures in the Main Ethiopian Rift, *Nature*, 297, 393-395,  
639 <https://doi.org/10.1038/297393a0>, 1982.
- 640 Asfaw, L. M.: Seismic risk at a site in the East African rift system, *Tectonophysics*, 209, 301-309,  
641 [https://doi.org/10.1016/0040-1951\(92\)90038-8](https://doi.org/10.1016/0040-1951(92)90038-8), 1992.
- 642 Asfaw, L. M.: Environmental hazard from fissures in the Main Ethiopian Rift, *Journal of African Earth Sciences*, 27,  
643 481-490, [https://doi.org/10.1016/S0899-5362\(98\)00074-8](https://doi.org/10.1016/S0899-5362(98)00074-8), 1998.



- 644 Asfaw, L. M.: Integrated approach to the study of geohazards with application in southern Afar, *Journal of African*  
645 *Earth Sciences*, 48, 237–244, <https://doi.org/10.1016/j.jafrearsci.2006.08.006>, 2007.
- 646 Ayalew, L. and Yamagishi, H.: Slope failures in the Blue Nile basin, as seen from landscape evolution perspective,  
647 *Geomorphology*, 57, 95–116, [https://doi.org/10.1016/S0169-555X\(03\)00085-0](https://doi.org/10.1016/S0169-555X(03)00085-0), 2004.
- 648 Ayalew, L.: Analysing the effects of historical and recent floods on channel pattern and the environment in the  
649 Lower Omo basin of Ethiopia using satellite images and GIS. *Environmental geology* 58, 8, 1713–1726,  
650 2009.
- 651 Ayalew, L., Yamagishi, H.: Slope failures in the Blue Nile basin, as seen from landscape evolution perspective.  
652 *Geomorphology* 57, 95–116, 2004.
- 653 Ayalew, L., Yamagishi, H., and Reik, G.: Ground cracks in Ethiopian Rift Valley: facts and uncertainties,  
654 *Engineering Geology*, 75, 309–324, <https://doi.org/10.1016/j.enggeo.2004.06.018>, 2004.
- 655 Ayalew, L., Möller, D.P. and Reik, G.: Using artificial neural networks (ANN) for real time flood forecasting, the  
656 Omo River case in southern Ethiopia. In *Proceedings of the 2007 Summer Computer Simulation*  
657 *Conference* (p. 19). Society for Computer Simulation International. 2007.
- 658 Ayele, A.: Probabilistic seismic hazard analysis (PSHA) for Ethiopia and the neighboring region, *Journal of African*  
659 *Earth Sciences*, 134, 257–264, <https://doi.org/10.1016/j.jafrearsci.2017.06.016>, 2017
- 660 Ayele, A., Jacques, E., Kassim, M., Kidane, T., Omar, A., Tait, S., Nercessian, A., de Chabalier, J. B., and King, G.:  
661 The volcano–seismic crisis in Afar, Ethiopia, starting September 2005, *Earth and Planetary Science Letters*,  
662 255, 177–187, <https://doi.org/10.1016/j.epsl.2006.12.014>, 2007.
- 663 Ayele, A., Keir, D., Ebinger, C., Wright, T. J., Stuart, G. W., Buck, W. R., Jacques, E., Ogubazghi, G., and Sholan,  
664 J.: September 2005 mega-dike emplacement in the Manda-Harraro nascent oceanic rift (Afar Depression),  
665 *Geophysical Research Letters*, 36, <https://doi.org/10.1029/2009GL039605>, 2009.
- 666 Ayenew, T. and Barbieri, G.: Inventory of landslides and susceptibility mapping in the Dessie area, northern  
667 Ethiopia, *Engineering Geology*, 77, 1–15, <https://doi.org/10.1016/j.enggeo.2004.07.002>, 2005.
- 668 Beyene, A. and Abdelsalam, M.G.: Tectonics of the Afar Depression: A review and synthesis. *Journal of African*  
669 *Earth Sciences* 41, 1-2, 41-59, 2005.
- 670 Billi, P.: Geomorphological landscapes of Ethiopia, In *Landscapes and Landforms of Ethiopia*, Springer, Dordrecht,  
671 3-32 pp., [https://doi.org/10.1007/978-94-017-8026-1\\_1](https://doi.org/10.1007/978-94-017-8026-1_1), 2015.
- 672 Billi, P. and Dramis, F.: Geomorphological investigation on gully erosion in the Rift Valley and the northern  
673 highlands of Ethiopia, *Catena*, 50, 353–368, [https://doi.org/10.1016/S0341-8162\(02\)00131-5](https://doi.org/10.1016/S0341-8162(02)00131-5), 2003.
- 674 Boccaletti, M., Mazzuoli, R., Bonini, M., Trua, T., Abebe, B.: Plio-Quaternary volcanotectonic activity in the  
675 northern sector of the Main Ethiopian Rift: relationships with oblique rifting. *Journal of African Earth*  
676 *Sciences* 29, 679-698, 2009.
- 677 Bolongaro-Crevenna, A., Torres-Rodríguez, V., Sorani, V., Frame, D., and Ortiz, M. A.: Geomorphometric analysis  
678 for characterizing landforms in Morelos State, Mexico, *Geomorphology*, 67, 407–422,  
679 <https://doi.org/10.1016/j.geomorph.2004.11.007>, 2005.
- 680 Bonini, M., Souriot, T., Boccaletti, M., Brun, J.P.: Successive orthogonal and oblique extension episodes in a rift  
681 zone: Laboratory experiments with application to the Ethiopian Rift. *Tectonics* 16, 347-362, 1997.
- 682 Bonini, M., Corti, G., Innocenti, F., Manetti, P., Mazzarini, F., Abebe, T., and Pecskey, Z.: Evolution of the Main  
683 Ethiopian Rift in the frame of Afar and Kenya rifts propagation, *Tectonics*, 24, 1–24,  
684 <https://doi.org/10.1029/2004TC001680>, 2005.
- 685 British Standard BS5930: Code of Practice for Site Investigations, British Standards Institution (BSI), London, 147  
686 pp., <https://doi.org/10.3404/00056552>, 1981.
- 687 Buriánek, D., Hroch, T., Verner, K., Megerssa, L., Martinek, K., Yakob, M., Haregot, A., Janderkova, J., Sima, J.,  
688 Krystofova, E., Valenta, J., Tadesse, E., Mosisa, A., Dalke, G., Legesse, F., Assefa, G., Pecskey, Z.,  
689 Hejtmanekova, P., and Krejci, Z.: Explanatory notes to thematic geoscientific maps of Ethiopia at a scale of  
690 1: 50,000, Map Sheet 0638-C2 Dila. Czech Geological Survey, Prague, 103 pp, 2018.
- 691 Centre for Development and Environment: Ethio GIS CD-ROM Database file system, University of Bern,  
692 Switzerland, 1999
- 693 Chang, K.-J., Chan, Y.-Ch., Chen, R.-F., and Hsieh, Y.-Ch.: Geomorphological evolution of landslides near an  
694 active normal fault in northern Taiwan, as revealed by lidar and unmanned aircraft system data, *Nat.*  
695 *Hazards Earth Syst. Sci.*, 18, 709–727, <https://doi.org/10.5194/nhess-18-709-2018>, 2018.
- 696 Chorowicz, J.: The east African rift system, *Journal of African Earth Sciences*, 43, 379–410,  
697 <https://doi.org/10.1016/j.jafrearsci.2005.07.019>, 2005.



- 698 Corti, G.: Continental rift evolution: From rift initiation to incipient break-up in the Main Ethiopian Rift, East  
699 Africa, *Earth-Science Reviews*, 96, 1–53, <https://doi.org/10.1016/j.earscirev.2009.06.005>, 2009.
- 700 Dhont, D. and Chorowicz, J.: Review of the neotectonics of the Eastern Turkish–Armenian Plateau by geomorphic  
701 analysis of digital elevation model imagery, *International Journal of Earth Sciences*, 95, 34–49,  
702 <https://doi.org/10.1007/s00531-005-0020-3>, 2006.
- 703 Ebinger, C. J., Yemane, T., Woldegabriel, G., Aronson, J. L., and Walter, R. C.: Late Eocene–Recent volcanism and  
704 faulting in the southern Main Ethiopian Rift, *Journal of the Geological Society*, 150, 99–108,  
705 <https://doi.org/10.1144/gsjgs.150.1.0099>, 1993.
- 706 Ebinger, C. J., Yemane, T., Harding, D. J., Tesfaye, S., Kelley S., and Rex D. C.: Rift deflection, migration, and  
707 propagation: Linkage of the Ethiopian and Eastern rifts, Africa, *Geological Society of America Bulletin*,  
708 112, 163–176, [https://doi.org/10.1130/0016-7606\(2000\)112<163:RDMAPL>2.0.CO;2](https://doi.org/10.1130/0016-7606(2000)112<163:RDMAPL>2.0.CO;2), 2000.
- 709 Erbello, A. and Kidane, T.: Timing of volcanism and initiation of rifting in the Omo–Turkana depression, southwest  
710 Ethiopia: Evidence from paleomagnetism, *Journal of African Earth Sciences*, 139, 319–329,  
711 <https://doi.org/10.1016/j.jafrearsci.2017.12.031>, 2018.
- 712 FAO, Food and Agriculture Organization, *Global Forest Resources Assessment 2000: Main Report*, FAO Forestry  
713 Paper 140, Rome, Italy, [https://doi.org/10.1016/S0264-8377\(03\)00003-6](https://doi.org/10.1016/S0264-8377(03)00003-6), 2001
- 714 Fisher, P., Wood, J., and Cheng, T.: Where is Helvellyn? Fuzziness of multi-scale landscape morphometry,  
715 *Transactions of the Institute of British Geographers*, 29, 106–128, <https://doi.org/10.1111/j.0020-2754.2004.00117.x>, 2004.
- 717 Fritz, H., Abdelsalam, M., Ali, K. A., Bingen, B., Collins, A. S., Fowler, A. R., Ghebreab, W., Hauenberger, C. A.,  
718 Johnson, P. R., Kusky, T. M., and Macey, P.: Orogen styles in the East African Orogen: a review of the  
719 Neoproterozoic to Cambrian tectonic evolution, *Journal of African Earth Sciences*, 86, 65–106,  
720 <https://doi.org/10.1016/j.jafrearsci.2013.06.004>, 2013.
- 721 Fubelli, G., Abebe, B., Dramis, F., and Vinci, S.: Geomorphological evolution and present-day processes in the  
722 Dessie Graben (Wollo, Ethiopia), *Catena*, 75, 28–37, <https://doi.org/10.1016/j.catena.2008.04.001>, 2008.
- 723 Ganas, A., Pavlides, S., and Karastathisa, V.: DEM-based morphometry of range-front escarpments in Attica, central  
724 Greece, and its relation to fault slip rates, *Geomorphology*, 65, 301–319,  
725 <https://doi.org/10.1016/j.geomorph.2004.09.006>, 2005.
- 726 Gao, M., Zeilinger, G., Xu, X., Wang Q., and Hao, M.: DEM and GIS analysis of geomorphic indices for evaluating  
727 recent uplift of the northeastern margin of the Tibetan Plateau, China, *Geomorphology*, 190, 61–72,  
728 <https://doi.org/10.1016/j.geomorph.2013.02.008>, 2013.
- 729 Gessesse D.: *Forest Decline in South Central Ethiopia Extent, history and process*. Doctoral dissertation.  
730 Department of Physical Geography and Quaternary Geology. Stockholm University, Sweden, 2007.
- 731 Gete, Z. and Hurni, H.: Implications of Land Use and Land Cover dynamics for mountain resource degradation in  
732 the northwestern Ethiopian highlands, *Mountain Research and Development*, 21, 184–191,  
733 [https://doi.org/10.1659/0276-4741\(2001\)021\[0184:IOLUAL\]2.0.CO;2](https://doi.org/10.1659/0276-4741(2001)021[0184:IOLUAL]2.0.CO;2), 2001.
- 734 Gezahegn A. and Dessie T.: Report on Engineering geophysical investigation of the Blue Nile basin for rerouting of  
735 the main road, Ethiopian Institute of Geological Survey, 1994.
- 736 Goitom, B., Oppenheimer, C., Hammond, J. O., Grandin, R., Barrie, T., Donovan, A., Ogubazghi, G., Yohannes, E.,  
737 Kibrom, G., Kendall, J. M. and Carn, S. A.: First recorded eruption of Nabro volcano, Eritrea, 2011,  
738 *Bulletin of volcanology*, 77, 85, 2015.
- 739 Gouin, P.: Kara Kore and Serdo epicenters: relocation and tectonic implications, *Bulletin of the Geophysical*  
740 *Observatory*, vol. 15, 15–25 pp., 1975.
- 741 Gouin, P.: *Earthquake history of Ethiopia and the Horn of Africa*, International Development Research Centre,  
742 Ottawa, Canada, 1979.
- 743 Habtamu, E., Ermiyas, F., Tutan, N., and Tsigezana, T.: *Engineering Geological Map of Dila Sheet at scale of*  
744 *1:250,000 scale (NB 37-6)*, Geological Survey of Ethiopia, Addis Ababa, 2012.
- 745 Hayward, N. J. and Ebinger, C. J.: Variations in the along-axis segmentation of the Afar Rift system, *Tectonics*, 15,  
746 244–257, <https://doi.org/10.1029/95TC02292>, 1996.
- 747 Hearn, G. J.: Slope hazards on the Ethiopian road network, *Quarterly Journal of Engineering Geology and*  
748 *Hydrogeology*, 2018–2058. 2018.
- 749 ISRM, International Society of Rock Mechanics Commission on Testing Methods: Suggested method for  
750 determining point load strength, *Int. J. Rock Mech. Min. Sci. and Geomech.*, 22, 51–60,  
751 [https://doi.org/10.1016/0148-9062\(85\)92985-7](https://doi.org/10.1016/0148-9062(85)92985-7), 1985.





- 752 Janetos, A. C., Justice, C. O.: Land covers global productivity: a measurement strategy for the NASA programme,  
753 International Journal of Remote Sensing, 21, 1491-1512, <https://doi.org/10.1080/014311600210281>,  
754 2000.
- 755 JICA and GSE: The Project for Developing Countermeasures against Landslides in the Abay River Gorge, technical  
756 report, Japan International Cooperation Agency and Geological Survey of Ethiopia, 348 pp., 2012.
- 757 Kopačková, V., Rapprich, V., Šebesta, J., and Zelenkova, K.: Slope dependent morphometric analysis as a tool  
758 contributing to reconstruction of volcano evolution, In Earth and environmental sciences, InTech,  
759 <https://doi.org/10.5772/29466>, 2011.
- 760 Kropáček, J., Vařilová, Z., Baroň, I., Bhattacharya, A., Eberle, J., and Hochschild, V.: Remote sensing for  
761 characterisation and kinematic analysis of large slope failures: Debre sina landslide, main ethiopian rift  
762 escarpment, Remote Sensing, 7, 16183-16203, <https://doi.org/10.3390/rs71215821>, 2015.
- 763 Kumar, V., Gupta, V., and Sundriyal, Y. P.: Spatial interrelationship of landslides, litho-tectonics, and climate  
764 regime, Satluj valley, Northwest Himalaya, Geological Journal, 54, 537-551,  
765 <https://doi.org/10.1002/gj.3204>, 2019.
- 766 Kycl, P., Rapprich, V., Verner, K., Novotný, J., Hroch, T., Mišurec, J., Eshetu, H., Haile, E. T., Alemayehu, L., and  
767 Goslar, T.: Tectonic control of complex slope failures in the Ameka River Valley (Lower Gibe Area,  
768 central Ethiopia): Implications for landslide formation, Geomorphology, 288, 175-187,  
769 <https://doi.org/10.1016/j.geomorph.2017.03.020>, 2017.
- 770 Lemessa, G., Asfaw, B., Mamo, S., and Ashenafi, S.: Mass movement hazards assessment on Betto and Sawla sub  
771 sheet of Goffa district, North Omo Zone, Southern Nations Nationalities and People's Regional State,  
772 technical Report, Geological Survey of Ethiopia, 2000.
- 773 Mancini, F., Ceppi, C., and Ritrovato, G.: GIS and statistical analysis for landslide susceptibility mapping in the  
774 Daunia area, Italy, Nat. Hazards Earth Syst. Sci., 10, 1851-1864, [https://doi.org/10.5194/nhess-10-1851-](https://doi.org/10.5194/nhess-10-1851-2010)  
775 [2010](https://doi.org/10.5194/nhess-10-1851-2010), 2010.
- 776 Meinhardt, M., Fink, M., and Tünschel, H.: Landslide susceptibility analysis in central Vietnam based on an  
777 incomplete landslide inventory: Comparison of a new method to calculate weighting factors by means of  
778 bivariate statistics, Geomorphology, 234, 80-97, <https://doi.org/10.1016/j.geomorph.2014.12.042>, 2015.
- 779 Melese, S. M.: Effect of land use land cover changes on the forest resources of Ethiopia, International Journal of  
780 Natural Resource Ecology and Management, 1, 51, <https://doi.org/10.11648/j.ijnrem.20160102.16>, 2016.
- 781 Muluneh, A. A., Cuffaro, M., and Doglioni, C.: Left-lateral transtension along the Ethiopian Rift and constrains on  
782 the mantle-reference plate motions, Tectonophysics, 632, 21-31,  
783 <https://doi.org/10.1016/j.tecto.2014.05.036>, 2014.
- 784 Peduzzi, P.: Landslides and vegetation cover in the 2005 North Pakistan earthquake: a GIS and statistical  
785 quantitative approach, Nat. Hazards Earth Syst. Sci., 10, 623-640, [https://doi.org/10.5194/nhess-10-623-](https://doi.org/10.5194/nhess-10-623-2010)  
786 [2010](https://doi.org/10.5194/nhess-10-623-2010), 2010.
- 787 Pike, R. J.: Geomorphometry-diversity in quantitative surface analysis, Progress in Physical Geography, 24, 1-20,  
788 <https://doi.org/10.1177/030913330002400101>, 2000.
- 789 Rapprich, V., Eshetu, H.: Geological hazards and engineering geology maps of Dilla NB 37-6, Czech Development  
790 Agency, Czech Geological Survey, Geological Survey of Ethiopia, 2014.
- 791 Rapprich, V., Erban, V., Fárová, K., Kopačková, V., Bellon, H., and Hernandez, W.: Volcanic history of the  
792 Conchagua Peninsula (eastern El Salvador), Journal of Geosciences, 55, 95-112,  
793 <https://doi.org/10.3190/jgeosci.069>, 2010.
- 794 Rapprich, V., Nida, D., and Bizuye, Y.: Geological hazards and engineering geology maps of Hossana NB 37-2,  
795 Czech Development Agency, Czech Geological Survey, Geological Survey of Ethiopia, 2014.
- 796 Saria, E., Calais, E., Stamps, D. S., Delvaux, D., and Hartnady, C. J. H.: Present-day kinematics of the East African  
797 Rift, Journal of Geophysical Research: Solid Earth, 119, 3584-3600,  
798 <https://doi.org/10.1002/2013JB010901>, 2014.
- 799 Sembroni, A., Faccenna, C., Becker T. W., Molin, P., and Abebe, B.: Long-term, deep-mantle support of the  
800 Ethiopia-Yemen Plateau, Tectonics, 35, 69-488, <https://doi.org/10.1002/2015TC004000>, 2016.
- 801 Tadesse, T.: Recent landslide and resulting damages in the Blue Nile River Gorge and its tributaries, Eastern Gojam  
802 Zone, Technical Report, Geological Survey of Ethiopia, 1993.
- 803 Temesgen, B., Umer, M., Asrat, A., Berakhi, O., Ayele, A., Francesco, D. and Demissie, M.: Landslide hazard on  
804 the slopes of Dabicho Ridge, Wondo Genet area: the case of June 18, 1996 event, SINET: Ethiopian  
805 Journal of Science, 22, 127-140, 1999



- 806 Temesgen, B., Mohammed, M. U., and Korme, T.: Natural hazard assessment using GIS and remote sensing  
807 methods, with particular reference to the landslides in the Wondogenet area, Ethiopia, *Physics and*  
808 *Chemistry of the Earth, Part C: Solar, Terrestrial & Planetary Science*, 26, 665-675,  
809 [https://doi.org/10.1016/S1464-1917\(01\)00065-4](https://doi.org/10.1016/S1464-1917(01)00065-4), 2001.
- 810 U.S. Geological Survey, Earthquake Hazards Program, Advanced National Seismic System (ANSS),  
811 Comprehensive Catalogue of Earthquake Events and Products: Various,  
812 <https://doi.org/10.5066/F7MS3QZH>, 2017.
- 813 Vařilová, Z., Kropáčěk, J., Zvelebil, J., Šťastný, M. and Vilímek, V.: Reactivation of mass movements in Dessie  
814 graben, the example of an active landslide area in the Ethiopian Highlands, *Landslides*, 12, 985-996,  
815 <https://doi.org/10.1007/s10346-015-0613-2>, 2015.
- 816 Verner, K., Megerssa, L., Buriánek, D., Martínek, K., Hroch, T., Yakob, M., Haregot, A., Bewketu, H., Mosisa, A.,  
817 Dalke, G., Hejtmánková, P., and Krejčí, Z.: Geological map at a scale of 1:50,000, Geological and thematic  
818 maps at a scale of 1:50,000 for Mejo, Leku, Arba Minch and Dila areas, SNNPR, Ethiopia. Czech  
819 Geological Survey, Prague, Map Sheet 0638-D2 Mejo, 2018a.
- 820 Verner, K., Megerssa, L., Hroch, T., Buriánek, D., Martínek, K., Yakob, M., Haregot, A., Janderková, J., Šíma, J.,  
821 Kryštofová, E., Valenta, J., Bewketu, H., Mosisa, A., Dalke, G., Assefa, G., Pécskay, Z., Hejtmánková, P.,  
822 and Krejčí, Z.: Explanatory notes to the thematic geoscientific maps of Ethiopia at a scale of 1:50,000,  
823 Czech Geological Survey, Prague, Map Sheet 0638-D2 Mejo, 2018b.
- 824 Verner, K., Megerssa, L., Hroch, T., Buriánek, D., Martínek, K., Gebremariyam, H., Tadesse, E., Legesse, F., Nisra,  
825 E., Abateneh, B., Hejtmánková, P., and Krejčí, Z.: Geological map at a scale of 1:50,000, Geological and  
826 thematic maps at a scale 1:50,000 for Mejo, Leku, Arba Minch and Dila areas, SNNPR, Ethiopia, Czech  
827 Geological Survey, Prague, Map Sheet 0637-D3 Arba Minch, 2018c.
- 828 Verner, K., Megerssa, L., Hroch, T., Buriánek, D., Martínek, K., Janderková, J., Šíma, J., Kryštofová, E.,  
829 Gebremariyam, H., Tadesse, E., Legesse, F., Nisra, E., Abateneh, B., Assefa, G., Valenta, J., Pécskay, Z.,  
830 Hejtmánková, P., and Krejčí, Z.: Explanatory notes to the thematic geoscientific maps of Ethiopia at a scale  
831 of 1:50,000, Czech Geological Survey, Prague, Map Sheet 0637-D3 Arba Minch, 2018d.
- 832 Wilks, M., Ayele, A., Kendall, J. M., and Wookey, J.: The 24th January 2016 Hawassa earthquake: Implications for  
833 seismic hazard in the Main Ethiopian Rift, *Journal of African Earth Sciences*, 125, 118-125,  
834 <https://doi.org/10.1016/j.afrearsci.2016.11.007>, 2017.
- 835 Williams, F. M., Williams, M. A. J., and Aumento, F.: Tensional fissures and crustal extension rates in the northern  
836 part of the Main Ethiopian Rift, *Journal of African Earth Sciences*, 38, 183-197,  
837 <https://doi.org/10.1016/j.afrearsci.2003.10.007>, 2004.
- 838 Woldearegay, K.: Review of the occurrences and influencing factors of landslides in the highlands of Ethiopia: With  
839 implications for infrastructural development, *Momona Ethiopian Journal of Science*, 5, 3-31,  
840 <https://doi.org/10.4314/mejs.v5i1.85329>, 2013.
- 841 Woldegabriel, G., Heiken, G., White, T. D., Asfaw, B., Hart, W. K., and Renne, P. R.: Volcanism, tectonism,  
842 sedimentation, and the paleoanthropological record in the Ethiopian Rift System, *Special papers-Geological*  
843 *Society of America*, 83-99, 2000.
- 844 Wolfenden, E., Ebinger, C., Yirgu G., Deino A., Ayale D.: Evolution of the northern Main Ethiopian rift: birth of a  
845 triple junction, *Earth and Planetary Science Letters*, 224, 213-228,  
846 <https://doi.org/10.1016/j.epsl.2004.04.022>, 2004.
- 847 Wood, J. D.: The geomorphologic characterization of digital elevation models, Ph.D. Thesis, University of  
848 Leicester, UK, 1996.
- 849 Wotchoko, P., Bardintzeff, J. M., Itiga, Z., Nkouathio, D. G., Guedjeo, C. S., Ngnoupeck, G., Dongmo, A. and  
850 Wandji, P.: Geohazards (Floods and Landslides) in the Ndop Plain, Cameroon volcanic nine, *Open*  
851 *Geosciences*, 8, 429-449, <https://doi.org/10.1515/geo-2016-0030>, 2016.
- 852 Xue, L., Alemu, T., Gani, N. D., and Abdelsalama, M. G.: Spatial and temporal variation of tectonic uplift in the  
853 southeastern Ethiopian Plateau from morphotectonic analysis, *Geomorphology*, 309, 98-111,  
854 <https://doi.org/10.1016/j.geomorph.2018.02.025>, 2018.
- 855 Yekoye, B., Yewubinesh, B., and Debebe, N.: Engineering Geological Map of Hosaina sheet (NB 37-2) at scale of  
856 1:250,000, Geological Survey of Ethiopia, Addis Ababa, 2012.
- 857 Zvelebil, J., Šíma, J., and Vilímek, V.: Geo-risk management for developing countries—vulnerability to mass  
858 wasting in the Jemma River Basin, Ethiopia, *Landslides*, 7, 99-103, [https://doi.org/10.1007/s10346-009-](https://doi.org/10.1007/s10346-009-0191-2)  
859 [0191-2](https://doi.org/10.1007/s10346-009-0191-2), 2010.



860 Zwaan F., Schreurs G.: Rift segment interaction in orthogonal and rotational extension experiments: Implications for  
861 the large-scale development of rift systems. *Journal of Structural Geology*, 140, 1-17,  
862 <https://doi.org/10.1016/j.jsg.2020.104119>, 2020.  
863